CHALMERS
UNIVERSITY OF TECHNOLOGY

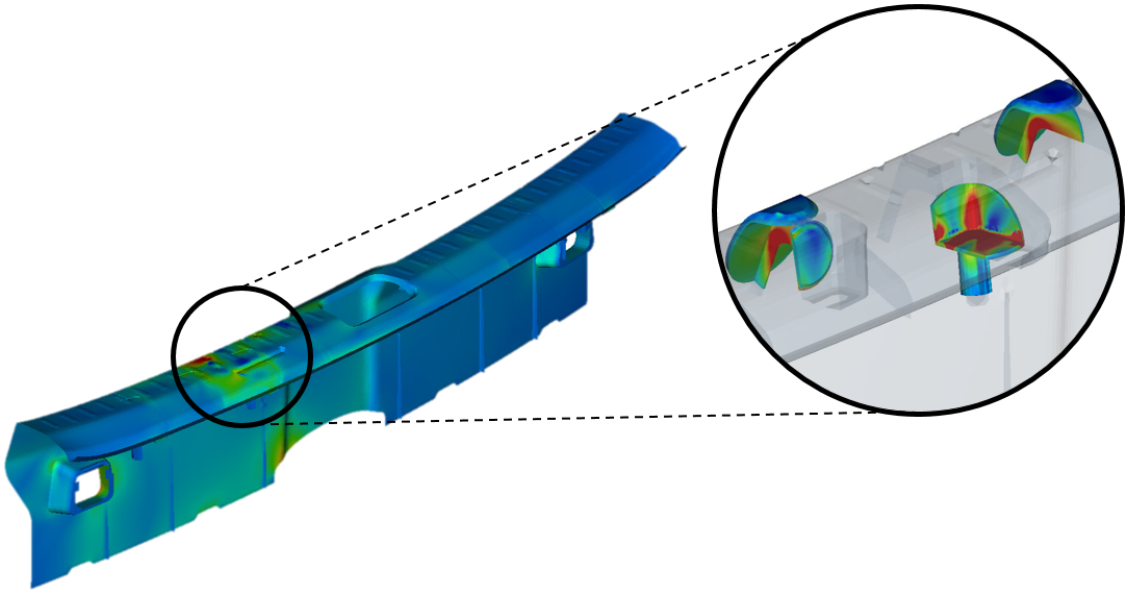

Method for merging scales in finite element analyses

Framework for automated global/local analyses

Master's thesis in the Master's programme Applied Mechanics

Carl Möller
Oscar Sundlo

Department of Applied Mechanics
Chalmers University of Technology
Gothenburg, Sweden 2017

Master's thesis 2017:28

Method for merging scales in finite element analyses

Framework for automated global/local analyses

Carl Möller & Oscar Sundlo

CHALMERS
UNIVERSITY OF TECHNOLOGY

Department of Applied Mechanics
Division of Material and Computational Mechanics
Chalmers University of Technology
Gothenburg, Sweden 2017

Method for merging scales in finite element analyses
Framework for automated global/local analyses
Carl Möller and Oscar Sundlo

Supervisor: M.Sc. Henrik Molker, Volvo Car Group
Examiner: Professor Leif Asp, Applied Mechanics

Master's Thesis 2017:28
ISSN 1652-8557
Department of Applied Mechanics
Division of Material and Computational Mechanics
Chalmers University of Technology
SE-412 96 Gothenburg
Telephone +46 31 772 1000

Cover: Strain response of a sillmoulding and three submodels in critical areas zoomed in.

Gothenburg, Sweden 2017

Method for merging scales in finite element analyses
Framework for automated global/local analyses
Carl Möller and Oscar Sundlo
Department of Applied Mechanics
Chalmers University of Technology

Abstract

The work of a CAE-engineer is a balance between accuracy and efficiency for the analyses. The outcome of the analyses must be accurate enough to be used for evaluation of the analysed component design and provide trustworthy recommendations when needed. Furthermore, it becomes increasingly important that the analyses are carried out fast to minimise lead time and cost. In today's work this balance is often met by choosing to rely on a coarser model together with engineering experience.

The aim of this thesis is to develop a method and provide guidelines for multiscale analyses that can be used to analyse critical areas in a global model with higher accuracy. This is done by adopting the technique of submodelling and developing a script to perform the steps of the method in an automatic manner.

Using the submodelling technique local models, also known as submodels, are created for critical areas found in the case studies. The new models are treated independently, only connected to the global analysis by applying new boundary conditions.

Several analyses where the submodel responses are evaluated using different modelling configurations, such as submodel size and element size, are performed. The outcome showed that, by using the submodelling approach, a more accurate response prediction can be made. Also, due to that the volumetric size is drastically reduced, this is achieved in a reasonable amount of time. Furthermore, is it concluded that the submodel volume must be chosen in such way that the boundaries of the volume are located where the strain concentration has subsided and that the submodel element size preferably is chosen even smaller than the recommended size used at Volvo Cars today. Finally, correlation to a physically tested component indicated that the submodels to a greater extent predicts damage as it showed up in the test, both in size and intensity.

The submodelling approach is automated in such way that the user of the script could interact with the submodelling process and make adjustment based on the specific geometry and load case.

Keywords: *Abaqus, Ansa, Meta, Submodelling, Multiscale analysis, Polymers*

Acknowledgements

This master's thesis is written by two students at Chalmers University of Technology, as the final part of the master's program in Applied Mechanics. The project was carried out during the spring semester of 2017 at the department of Durability - Body and Trim at Volvo Cars in Gothenburg.

First of all, we would like to thank our supervisor M.Sc. Henrik Molker and our examiner Prof. Leif Asp at Chalmers University of Technology for their expert advise and great feedback response.

Also, we would like to thank PhD Annika Lundberg and the group Durability - Body and trim at Volvo Cars for providing us with a friendly and motivating working environment.

Gothenburg, June 2017

Carl Möller & Oscar Sundlo

Terminology

.inp	- File format for input files in Abaqus.
.odb	- File format for output files in Abaqus.
Abaqus	- Commercial software FE-solver developed by Simulia™.
Ansa	- Commercial pre-processing software developed by Beta™ CAE Systems.
CAD	- Computer Aided Design.
CAE	- Computer Aided Engineering.
FEA	- Finite Element Analysis, see FEM.
FEM	- Finite Element Method, numerical calculation method to approximate solutions of partial differential equations.
GUI	- Graphical User Interface.
Meta	- Commercial post-processing software developed by Beta™ CAE Systems.
Python	- High-level programming language.
VCC	- Volvo Car Corporation.

Table of Contents

1 Introduction

To evaluate the strength of new car designs long before physical prototypes are available, Finite Element (FE) models are used. These models often include a large part of the car body to enable analysis on system level. Figure 1 shows the size of a model used to evaluate the strength of the rear sillmoulding. Consequently, due to the large size of the models the FE-modelling becomes a balance between accuracy and computational efficiency. Not seldom this leads to large models with a relatively coarse mesh of shell elements, in the order of 3-5 mm, to save computational cost.

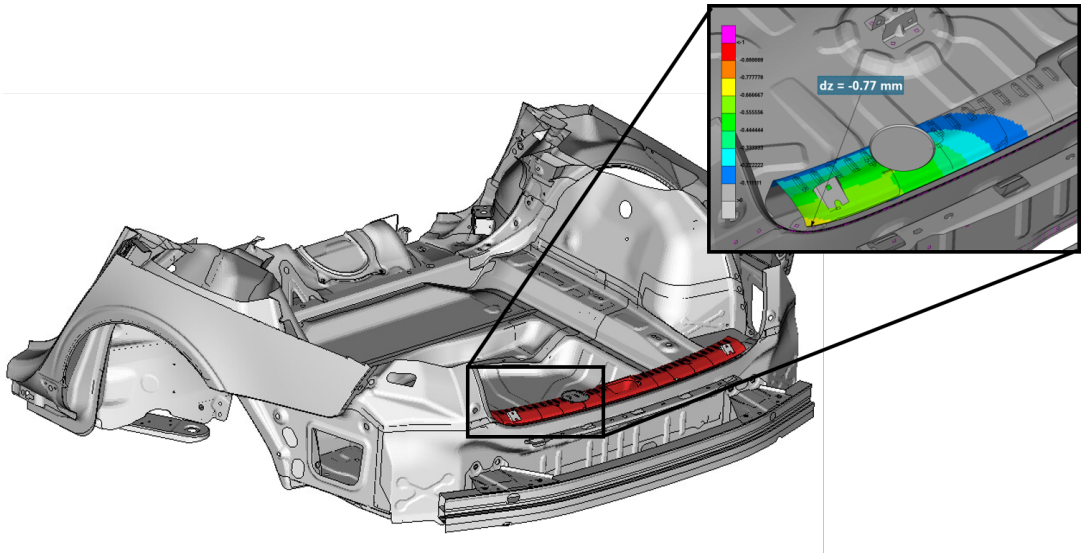

Figure 1: Global shell FE-model used to evaluate strength and stiffness of the trunk lid sillmoulding (marked red).

The mesh size used results in information loss of the true geometric details. One example is loss of the true radii representations at notches, such as T-junctions, with the consequence that the predicted stress- and strain-state in these areas becomes inaccurate. Another source of error by modelling with only shell elements is that the strains are in general underestimated compared to using solid elements [1].

In accordance to Volvo Cars modelling guidelines for polymers [2], submodels with solid elements are recommended for analyses of critical areas containing stress and strain concentrations in order to better predict the responses. This is a time consuming procedure, and it is often judged to be more effective to rely on only the result from the coarse mesh combined with the CAE-engineers experience.

1.1 Purpose

The aim of this project is to develop a multiscale modelling method and provide guidelines for submodelling of critical locations in global models in an automated process. This includes identification and refined computations of critical areas, hotspots, meaning a more efficient multiscale analysis method with less user interaction.

The purpose of the multiscale modelling method is to increase the accuracy of the final simulation results and thereby improve the evaluation of the design. Accordingly documented recommendations, on how to improve the component, can be more easily provided. All this should be done in an efficient manner, reducing the manual work to a minimum and keeping the computational cost low.

To achieve this purpose the following research questions must be answered:

1. Is it possible to use submodelling to obtain a more accurate solution?
2. What and how large is the difference in result between the global model and the refined submodel?
3. How much time can be saved by automating the method compared to perform the steps manually?

1.2 Limitations

The thesis is aimed at modelling of isotropic polymer materials. However, the long term purpose of the multiscale modelling method is to be extended to cover anisotropic materials, such as composites. The scale of models for accurate prediction of failure in composite materials must be of the size of the ply thickness, which is not feasible on a global level [3]. Material models and design data coupled to these will not be verified by testing. These are assumed to be known from the material database at Volvo Car Corporation (VCC) [4]. The fact that the material data for the polymers are time and temperature dependent will not be taken into consideration.

Correlation towards physical testing will be performed to validate the improvement of the method's result. The method will only be applied to a limited number of case studies with different geometries. All global modelling will be done according to VCC guidelines. There are today no general guidelines for submodelling. Finally, the method will be implemented in already available software used at VCC, mainly Abaqus as solver, and Ansa/Meta for pre/post-processing respectively.

1.3 Approach

In order to meet the aims of the project and to be able to quantify the effects of using a local submodelling technique a methodology and approach concerning the different steps of the analysis process illustrated in Figure 2 is considered.

It is crucial to identify the major steps in the current modelling process. The possibilities of how to implement and connect an enhanced submodelling process into the current process is then investigated. For this purpose, a literature study of the submodelling technique and the implementation possibilities is performed. As the project is handed out by VCC this also includes a study of their current standards regarding modelling, choices of design criteria and other guidelines treating polymers. The framework of the submodelling process can be divided into five steps; solve global model, identify critical locations (hot-spots), re-model critical locations with the true geometry representation (CAD-file), analyse the submodel's response

and correlate the analysis with physical testing of the component. These steps do also summarise the total methodology workflow, see Figure 2.

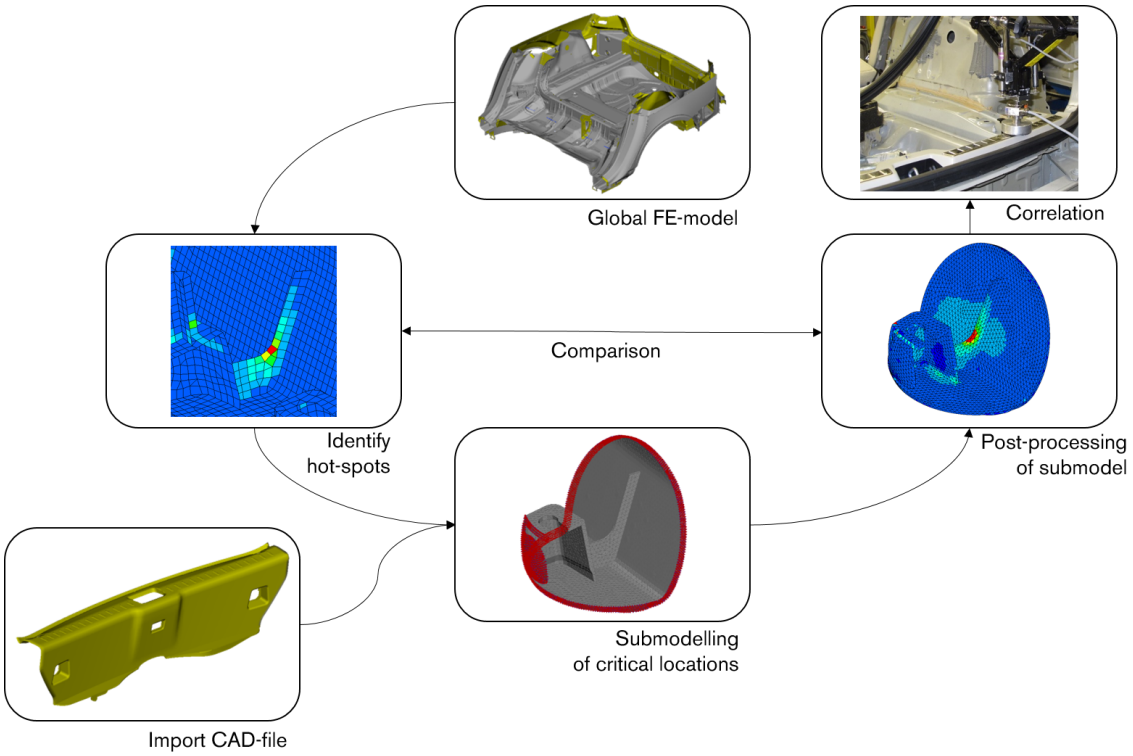

Figure 2: Flowchart of the proposed submodelling process.

The identified submodelling approach is applied on a reference load case, with a simple geometry, developed to study influences of different element types, sizes of submodel volume, etc. All modelling is performed using the pre-processor software Ansa version 17.0.1. The FE-solver Abaqus version 6.14-3 is used for all simulations and the post-processing is preformed in Meta version 15.3.3.

The submodelling approach is also applied to more complex models and load cases that are used by VCC today. These analyses are performed to detect further difficulties that appears when the different steps of the process are applied on more complex geometries. Examples of this is for instance effects of contact and couplings between parts that occur inside the extracted sub-volume domain.

To validate the efficiency and accuracy of the submodelling approach correlation towards a physical test is performed. The experimental tests have already been carried out in conjunction with earlier correlation work of the global model at VCC. However, the test response can now also be compared to response of the submodels.

The different modules of the submodelling methodology are coupled together into an automated process by developing Python scripts capable to perform the steps. The scripting is performed in such way that different modules can be easily changed and replaced for different applications. Three different scripts are developed; one script for post-processing of the initial global model, one script for pre-processing

of the submodels and one script for post-processing of submodels and comparison between submodels and global model results.

Each script consists of several functions that execute different steps of the modules in the submodelling approach. The functions have different input/outputs enabling different implementation configurations of modelling and post-processing, e.g different kind of design criteria. The scripting is done in the Ansa and Meta scripting toolboxes.

2 Theory

In the rapidly changing car industry it is crucial to keep lead times short. To attain a short lead time in the design process stage it is important that the feedback loop between the designer and the CAE engineer is quick. Therefore it is common to model on a global scale with a coarse shell element mesh, leading to suffering accuracy in the response in certain areas. However, the overall global FE-approximation response is often sufficiently accurate. Thus, refined calculations on a global level are unnecessary but may be needed locally for a better prediction of the stresses and strains used to verify that the specific component fulfil the requirements.

Traditional and well developed methods to locally improve the accuracy in a simulation are often based on refinement of the mesh in critical areas within the global model. These methods are categorised as coupled approaches as the locally refined mesh is coupled to the global mesh by introducing new constraints in between them [5]. The refinement can be done in an adaptive manner either by refining the mesh size or by increasing the regularity of the elements where the estimated error of the FE-model is large [6] (see e.g. Figure 3a). Similarly, when locally changing the scales from shells to solids, further constraints must be introduced, increasing the complexity and also the computational effort. One example on such constraints are shell-to-solid couplings.

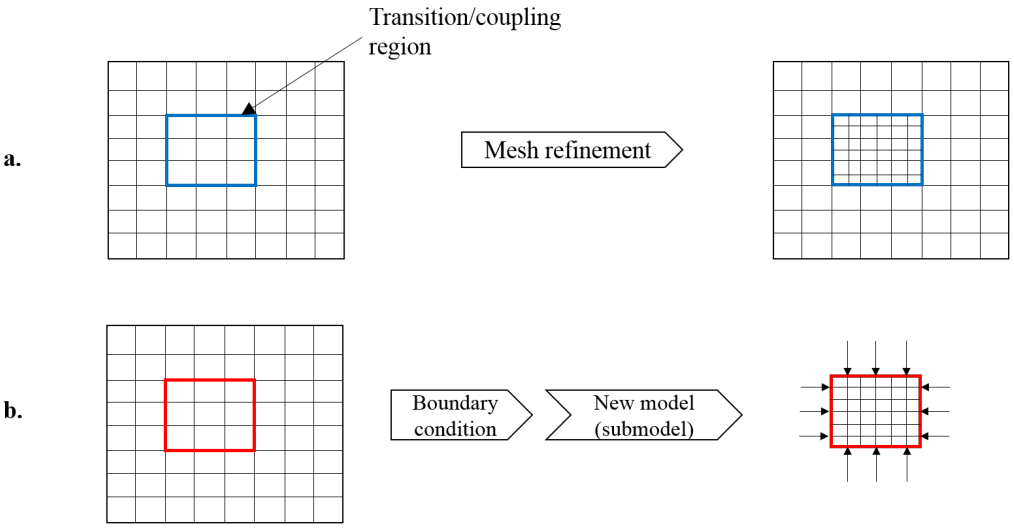

Figure 3: Different approaches for enhanced local calculations. a) Coupled approach and local mesh refinement within global model. b) Uncoupled approach with result extraction applied as boundary condition on submodel.

Coupled approaches are simple to implement and advantageously results in only one model that has to be built and solved, Figure 3a. This means that the refined local domain, as an included region in the global model, cannot be treated independently. The method also relies on that the connector/transition region, to merge the different scales between global and local domains, is modelled correctly to treat phenomena like "hanging nodes" [7] etc. Furthermore, another problem with modelling subdomains in a global model is that artificial stresses are introduced

at the intersected boundaries between the subdomain and the global model. This phenomenon can be handled using so called Multi-Point Constraints (MPC), which reduce artificial stresses and strains at the boundaries. However, the MPC methods often become difficult to implement for more advanced materials [5]. MPC is today implemented in many FE-applications, e.g. in Abaqus [8].

Another method for refining a global model locally is *ad hoc* where the shell elements in the area of interest are replaced by 3D solid elements. The solid elements can then be coupled to the surrounding shell elements in two different ways. Either by using the Mindlin-Reissner kinematic assumptions of the shell elements to formulate the coupling between the 2D and 3D elements. The other approach is based on a higher order formulation of the shell elements that allows stretching of the thickness [9]. The *ad hoc* method using the Mindlin-Reissner kinematic assumptions causes unrealistic high stresses where the two different element types are connected. By using the higher order element the overestimation of the stresses can be reduced [5].

Instead of imposing additional constraints only at the boundary between the global and local mesh, more advanced techniques have recently been developed allowing for a more natural transition. One of those techniques is the so called Mesh Superposition Technique (MST) [5][10]. Using MST the different scale meshes (global and local) are overlapping over a small area where the total stiffness and mass contributions are weighted together from respective part, Figure 4. Gigliotti and Pinho [5][10] show that the technique can be advantageous as unwanted stress disturbances becomes infinitesimal, allowing to make the local area even smaller. In the latter work the mathematical explanation of the technique is given. So far the approach is not implemented in any commercial FE-software.

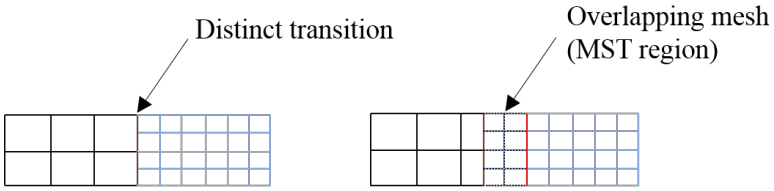

Figure 4: Transition possibilities for coupling different scales.

If the constrain equations, for either of the described methods, are known they can often be easily implemented and advantageously gives only one model. However, to completely eliminate the need of connector elements/regions, an uncoupled method using locally created submodels is an alternative [11], see Figure 3b.

2.1 Submodelling

Submodelling is a technique for creating local models, submodels, only representing a small part of the total structure included in the global model. Using this technique local phenomena, where the global model was insufficiently accurate, can be captured in a second analysis. The approach of cutting volumes of interest into smaller substructures has shown to be advantageous by keeping the computational time down when performing refined calculations on the new model [12]. Higher accuracy

in the submodels can either be achieved by refining the scales in the submodel, i.e. going to smaller elements, or by going from 2D shell elements to 3D solid elements, which is necessary if all geometrical features should be captured[1]. Unlike the traditional approaches, the submodels can be treated as independent computational models, only driven by the response of the global model used as boundary conditions, see Figure 3b. This eliminates the need of a correctly modelled transition between the global and local mesh. However, there could still be response disturbances at the boundaries. Another benefit following from the fact that the submodel is a separate subsystem is that the global model can be solved just once and then be used to drive several submodels. This allows for fast and efficient optimisation of the design in the critical area, only by reproducing the local model simulation provided that the changes are small to not effect the global stiffness properties. However, by inducing a two stage approach to first solve the global model and then the local submodels, the analysis process becomes more challenging in handling both models and motivates for further research in the area.

The method of submodelling is based on St. Venant's principle stating that effects, such as stress concentrations, only occurs locally [13]. Such stress concentrations may constitute structural hot-spots, which merit further study. Therefore, the boundaries for a statically equivalent subsystem safely can be drawn at a distance from the hot-spot, where the loads of the global model are accurate. This distance from the hot-spot, where the model is cut to achieve a representative submodel, also known as attenuation length (la), is highly dependent on the geometric representation of the structure and contact regions [14]. Krueger and O'Brien [15] analysed the influence of the submodel size on predicted delamination criticality for composites loaded in bending. In this context they showed that already at a distance three thicknesses away from the delamination front the response was accurate within 1% compared to a full solid model. Also, for cylindrical components such as pressure vessels, this length can be approximated as [14]

$$la = 1.25 \cdot \sqrt{R \cdot t} \tag{1}$$

where R is the radius of the cylindrical vessel and t the membrane thickness. To the authors knowledge there are no general rules on the attenuation length for submodel generation.

Despite that the method of using submodels almost always has showed similar accuracy and reduced the computational cost compared to modelling using a global model with similar mesh resolution [12] the usage of submodelling today is limited. This is due to the fact that it requires further modelling and analysis of both a global model and submodels. Instead the analysis relies on engineering judgement, experience and by putting more narrow conditions on the component design where uncertainties exist. Some of the most commonly used design criteria for judging a component design are presented in Section 2.2.

[1]For composites a solid representation often is crucial to achieve an accurate FE-approximation [3].

2.1.1 Submodelling techniques

In general two approaches exist for creating the submodel and transferring the results from a global model to it's submodels; node-based and surface-based submodelling, which both are implemented in Abaqus [16].

The node-based approach is the simplest one and therefore also the most widely used technique for submodelling [16]. The approach implies that the boundaries of the submodel are driven from the nodes at the intersected boundaries. Most commonly by prescribing node displacements from the global results. In Figure 5 the technique is shown where the node displacements at the submodel boundary are mapped and interpolated from nodes that lies within a prescribed search distance in the global shell model [16]. Consequently, this approach is applicable if the meshes in the global and local model are of different types, e.g. shell-to-solid modelling. The translations and rotations in the global shell model are then translated to pure translations in the solid submodel.

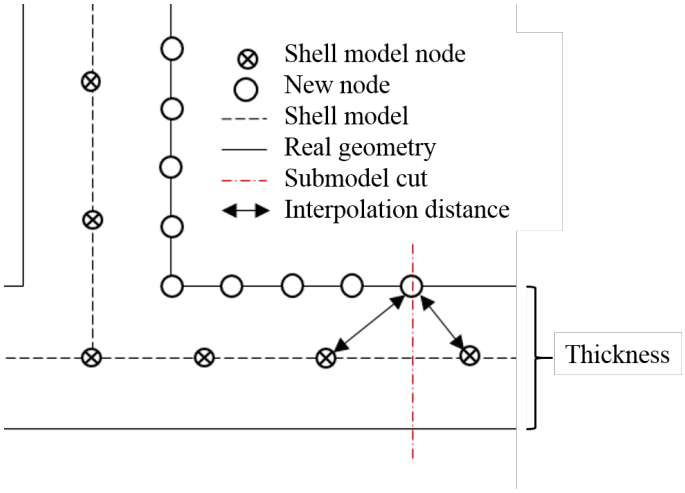

Figure 5: Node-based mapping of node results used as boundary condition in local model. Figure based on [16].

The second approach, surface-based submodelling, is to apply the boundary conditions as traction forces to the boundary surface of the submodel. That is, instead of the displacements the stress state of the global model is extracted and applied to the submodel. This approach requires that both the global and local model uses 3D solid element [16] which is seldom possible for the applications at VCC and hence only node-based modelling will be considered further on.

2.2 Design criteria

Depending on the material and the component application VCC today uses different design criteria. The criteria are used to determine if the design fulfils the requirements of the component or not. The requirements of the components are based on durability-, safety- and holistic design properties.

2.2.1 First principle strain design criterion

The most common design criterion in stiffness and strength analyses of polymers at VCC is to compare the first principal strain to the maximum allowable design strain of the material. Due to the properties of polymers, such as creep, the design allowable is specified dependent of the load situation, see Table 1. The allowable design strain for short term loading is according to the VCC standard set to be 70% of the ISO527 yield strain[2]. At critical locations where shell elements cannot capture the correct behaviour, the design criterion is reduced with a further safety margin of 50% [2]. If the strain in any radii exceeds 50% of the allowable design strain the result should be reported as an underestimation and the design be marked as NOK. This, unless the radius and the surrounding area has been further analysed, e.g. remodelled with solid elements.

Table 1: Design strain levels used for polymer analyses at VCC [4].

Loading	Design strain, ε_{d} [%]	Comment
Static short term	$\approx 2.0 - 5.0$	70% of ISO527 yield strain
Static long term	≈ 0.3	Critical strain level for micro cracks
Dynamic	$\approx 0.3 - 1.0$	-
Fatigue	$\approx 0.4 - 1.0$	Design strain at 10^6 cycles

2.2.2 Other design criteria

In certain applications the maximum displacement must be considered to ensure that the components do not come into contact or results in any visual and unwanted gaps. There may also be dynamic requirements of the design. In such cases requirements of the eigenfrequencies can be stated, e.g. to avoid resonance [2].

2.3 Polymer components

Many car components are manufactured in polymer materials. In general polymers have low density and are easy to form into complex shapes. On the other hand many polymers behave highly non linear, have relative low load carrying capacity and easily deforms plastically [17]. This means that load carrying polymer components needs to be strengthen structurally, e.g. by introducing so called reinforcing rib-structures, in order to meet all requirements. Figure 6 shows typical rib-structures on a component. To avoid manufacturing defects, such as shrink marks at the component surface, the ribs need to be thin (in the order of 1-3 mm), resulting in sharp radii at the attachment to the base surface. These radii easily causes stress/strain concentrations which may initiate cracks due to high loading.

[2]First point of zero secant stiffness for the material.

Figure 6: Rib structure underneath the rear door sill mould.

In Figure 7, the stress-strain curves for Acrylonitrile butadiene styrene (ABS) and Polypropylene (PP) at a temperature of 23°C are plotted[3]. The different material responses have a significant effect on the design criteria, especially when reducing the allowed strain level in shell models. For the ABS material this means that the maximum allowable stress is halved, from 40 MPa to 20 MPa according to Figure 7. Thus the material cannot be utilised to its full potential in analyses using shell elements if the design recommendations shall be used. This phenomenon further motivate why solid modelling is desirable.

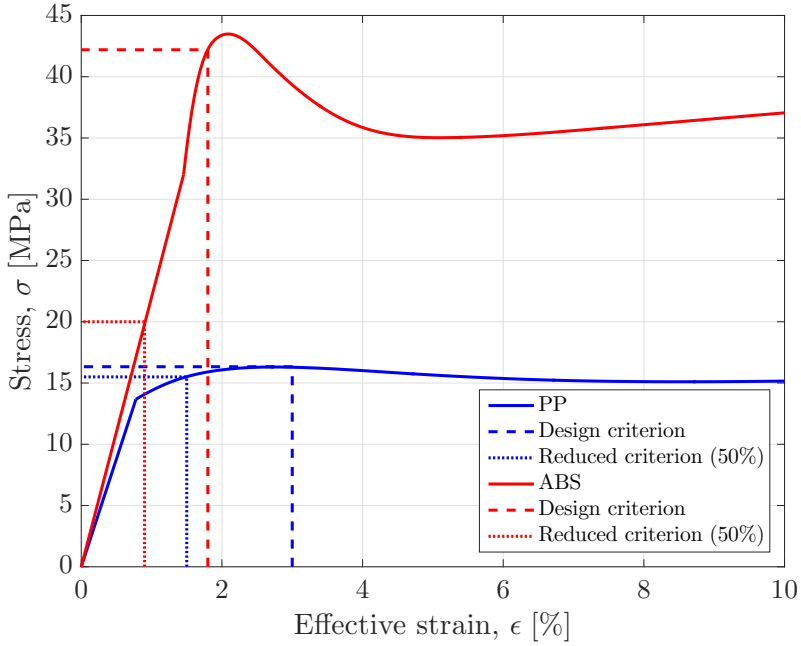

Figure 7: Stress-strain response for PP and ABS at temperature 23°C. Including the allowable design strain for static short term loading.

[3]Data from VCC material database.

2.3.1 Crazing

The most common micro damage type for thermoplastic polymer components is crazing which occurs when the material is loaded above the critical strain, $\varepsilon_{\text{crit}}$. This is the strain limit under which no plastic damage occurs, no matter for how long the material is subjected to the load. If the material is subjected to a load with a resulting strain response that exceeds $\varepsilon_{\text{crit}}$ crazing will occur and micro cracks are initiated. The micro cracks, also known as pseudo cracks, consist of elongated unidirectional molecular chains [17]. This often give rise to so called white marks which are distinguished by a change in colour at the component surface, see Figure 8. In Section 5 the material yield limit is used as an indication when crazing occurs and white marks have started to emerge.

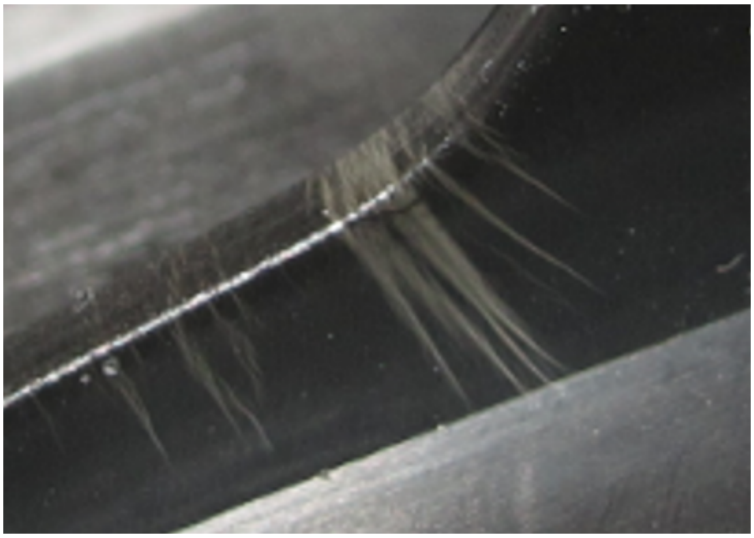

Figure 8: Crazing at a component made of ABS.

3 Process formulation

With the techniques and possibilities described in Section 2 in mind the total process can be identified, including both the current analysis with a global shell model and the added submodelling steps. A schematic of the process formulation is illustrated in Figure 9. The process is decomposed into different modules. For each of these the requirements regarding input and output data is specified. If some areas in the global model do not fulfil the design criteria for the designated application the critical areas should be re-modelled. The total submodelling process is further described in the following sections. A detailed user manual for the automation script is found in Section 6.

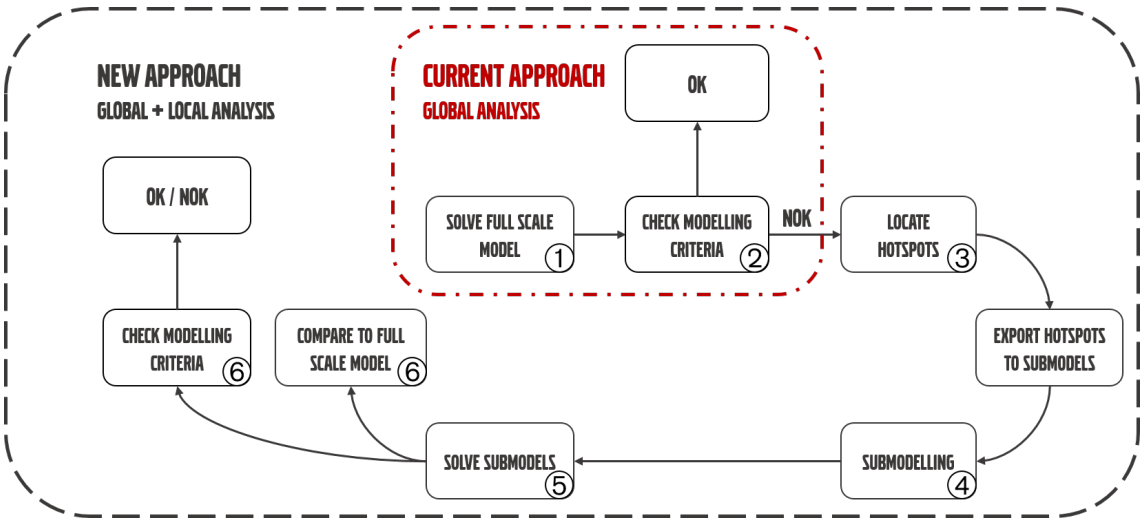

Figure 9: Schematic of the major steps in how an FE-problem is handled today compared to the enhanced method.

The global model needs to be constructed, solved and analysed to allow the CAE engineer to identify critical areas and hot-spots. The global modelling includes application of the correct boundary conditions, materials and mesh properties. With the current analysis methodology at VCC, i.e the steps in the dot-dashed red-lined box in Figure 9, it is after these steps the analysis stops and the result from the global analysis are used for the final OK/NOK-evaluation of the design. However, this part of the process is not new and must always be done regardless if the submodelling approach should be used or not. Thus, the global model is assumed to exist ① (Figure 9) as a prerequisite for this thesis work. Hence, no further development of the global modelling step is done in this thesis work and no further description of the global model step is given here. The interested reader is advised to see VCC documentation [18] or [2] for more information regarding global modelling. When solving the global model it is recommended to use full output precision in the FE-solver for the global model results. In this way numerical errors in the obtained submodel solution can be minimized. More details of this procedure are given in Appendix D.1.

After the global model has been solved the result is imported to the post-processor where the response and the design of the component of interest is analysed and

evaluated according to a known design criterion for the used material and load case ②. The design criterion is used to find critical locations, hot-spots, where the result exceeds the allowable value ③. These locations are subject for further analysis and submodels are constructed for these areas.

Importing the coordinates of the hot-spots into the pre-processor together with the original CAD-geometry of the model a new volume is created around each hot-spot ④. To avoid singularities, St.Venant's principle [13] is considered defining the submodel volume domain. Consequently, the submodel boundaries are introduced in regions where the stress or strain gradients are small as is illustrated in Figure 10. Also, it is necessary to make sure that the boundaries not are located too close to other surfaces, joints or kinks of the initial geometry. Such geometrical interference may cause problems when intersecting or meshing the volume in a later step. If the boundaries cannot be drawn without interfering with other areas of high stress/strain concentrations or geometrical complexities, it is preferable to consider a larger submodel that includes two hot-spots or more.

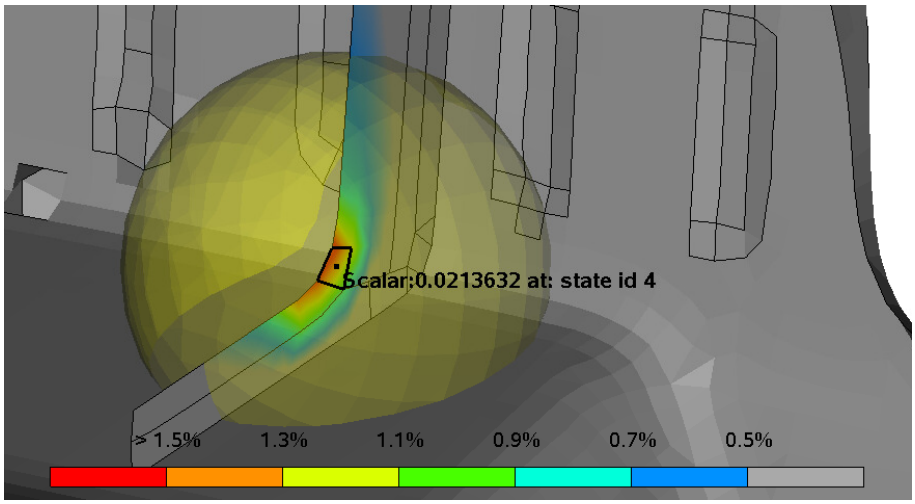

Figure 10: Spherical submodel volume definition in Meta. Shown result: first principal strain.

Parts outside the selected volume domain are removed by intersecting the new volume from the rest of the geometry ④. A set containing the intersected faces is created and assigned with submodel boundary conditions, see Figure 11. In the case of a global shell model and a solid submodel the boundary conditions must be configured as shell-to-solid. Consequently, when defining the boundary conditions, the shell thickness of the global model needs to be specified. This is required to assign the correct deformations in the global shell model to the correct nodes in the solid submodel by interpolation, see Figure 5. For fully comparable responses the driven boundary condition must subsequently be defined for each load step which was also used in the global analysis. The submodel is subsequently meshed with an appropriate element type and mesh size to obtain the desired geometry resolution, see Section 4.2.3.1. The submodels are solved by referring to the global solution file when starting the simulation ⑤.

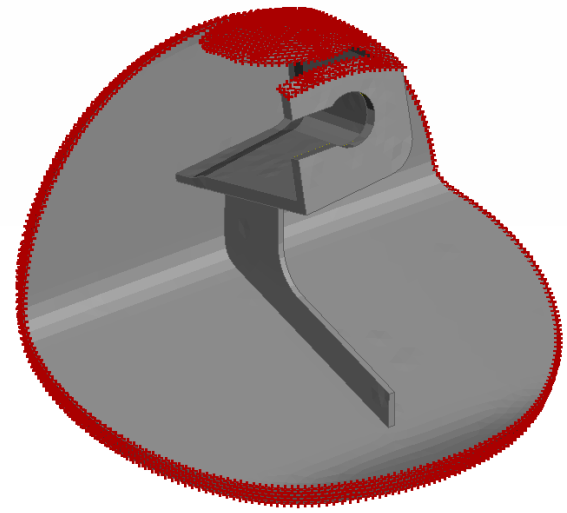

Figure 11: Driven nodes in the submodel marked red on the intersected boundaries.

If the submodel volume contains coupling constraints, joints or parts that may come into contact with each other this has to be taken into consideration in the submodelling process ④, see Section 4.2.2. One alternative is to merge all geometrical parts that lie within the submodel volume, i.e. not only consider the desired component of study but also include surrounding components. The coupling constraints and/or contact conditions are then recreated between the parts. This is illustrated in Figure 12a where A is the component of study and B is the connected component. Another way is to detect the areas of the submodel in which the coupling constraints and contacts are initiated and mark the corresponding surfaces as driven sets to inherent the results from the global model, Figure 12b.

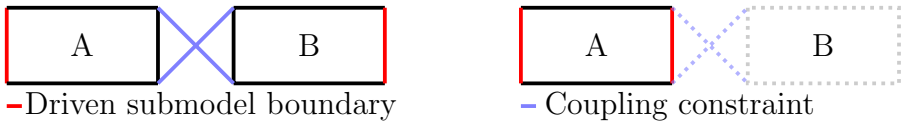

(a) Include couplings

(b) Exclude couplings and move the driven boundary

Figure 12: Alternatives to handle couplings in relation to the submodel when interested to study component A further.

When the submodels have been successfully solved they are post-processed and the results are compared to the results from the global analysis ⑥. The evaluation of the submodels should be preformed using the true design criteria. By checking the design criteria in the hot-spot regions the differences between the models can be identified and the designs can be evaluated. It is of interest to see if the submodels identify the critical points at the same locations or if new hot-spots are introduced with the enhanced modelling. Note that stresses and strains at the submodel boundaries can become inaccurate as a consequence of the prescribed boundary conditions, see Section 4.1.4. The result at the boundaries should therefore not be taken into consideration when evaluating the design. Also, it is important to identify results

that differ considerably between the global and local models. If a large deviation is observed this is most likely due to some coupling constraint, contact or loads from the global model are missed in the submodel, which therefore must be re-modelled.

As a further step in the post-process correlation to physically tested components can be performed for validation of the efficiency of the submodelling approach, done in Section 5.

4 Submodel analyses and results

In this section the submodelling approach described in previous section is applied in two case studies. The first case is a reference load case which allows for identification of problems caused by the procedure. Some identified consequences of the submodelling are further investigated by analysis of the remaining case. These analyses also concern a comparison between the global shell modelling and local solid modelling responses. The models used in the case studies are presented in detail in Appendix A.

4.1 Reference load case

To motivate and test the submodelling methodology defined in Section 3 and to compare the global and local model responses a reference case is analysed. The reference case covers a T-shaped geometry loaded in bending as illustrated in Figure 13.

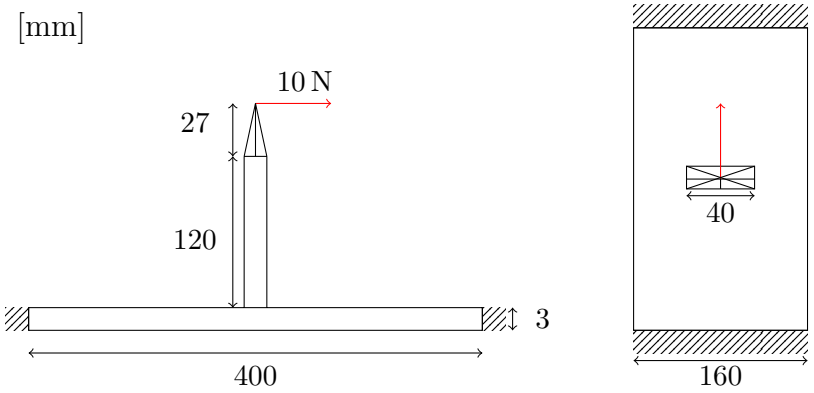

Figure 13: Reference load case of a rib loaded in bending. The force (red) is applied at a node 27 mm above the structure and connected to the structure using rigid elements. The boundaries are fixed (dashed area).

The reference load case is modelled in nine different configurations; two shell models using different T-junction casting techniques, described in Appendix A (Figure A.2), four global solid models and three solid submodels. The submodel geometry is modelled with a spherical volume with the hot-spot found in the global shell analyses, Point 1 in Figure 14, in the origin and a sphere radius of 60 mm.

In the following sections simulation time and strain response for the different models are compared. The full data is given in Appendix C. All simulations were run on the same server using 16 CPUs. The compared simulation time is the so called wallclock time, i.e. the time from that the FE-solver starts the job until it is completed. The design was evaluated by comparing the predicted maximum first principal strain, $\varepsilon_{1,\max}$ to the allowable design strain, assuming static short term loading. The allowable strain level for the ABS polymer is 1.8%[4] and reduced by 50% to 0.9% in shell model radii.

[4]From VCC material database. Material: Styrolution Terluran GP-22

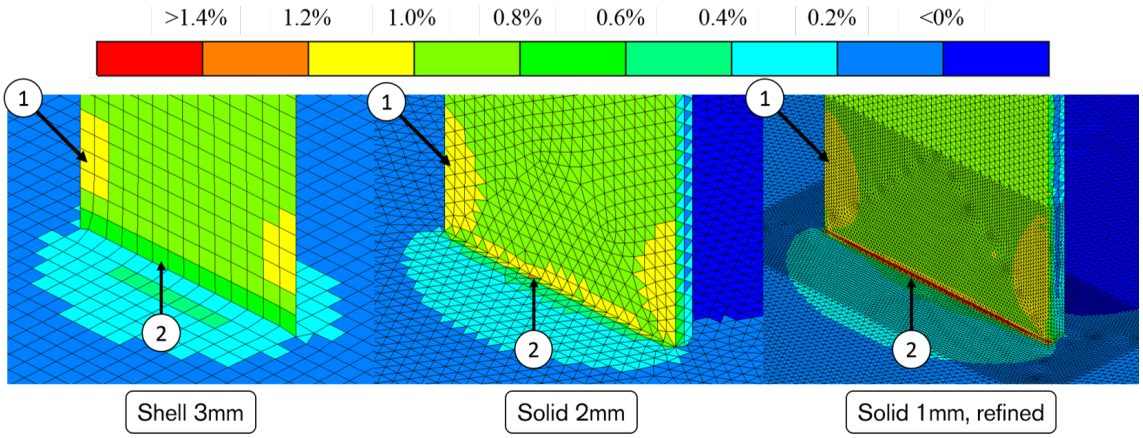

Figure 14: First principal strain distribution for global shell and solid models.

4.1.1 Time differences

Simulation times for analyses of the different model configurations are presented in Figure 15. The simulation for the shell models finish in only a few seconds while the solid models require significantly more computational time. The effect becomes more pronounced with an increase in number of elements, Figure 16. Also, comparing the effect of mesh density for the solid configurations, both global and submodels, it is seen that a small change in element size (1 mm difference) cause a huge increase in computational effort and the simulation time more than doubles. Overall the submodels reduced the simulation times to 20-30% of the time used for the solid global model meshed with the same element size, e.g. for 1 mm elements it took 255 sec compared to 1218 sec.

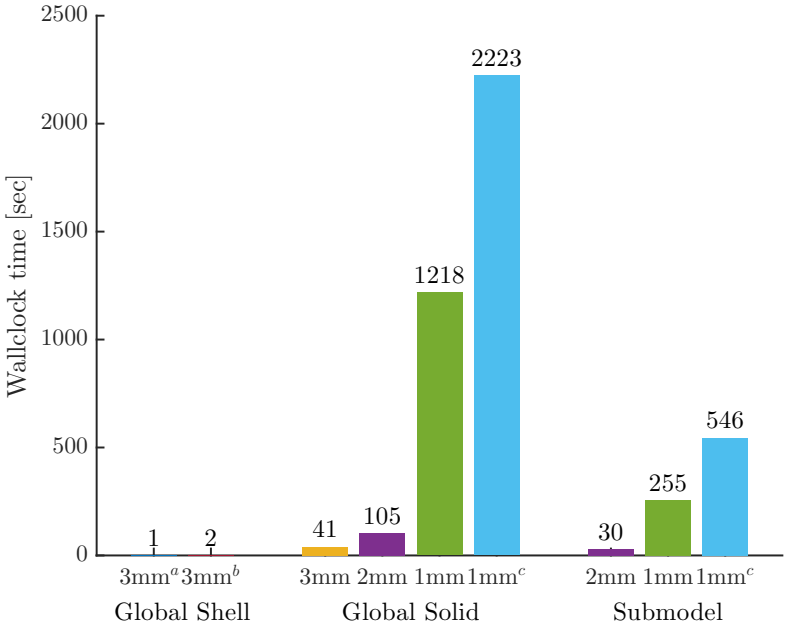

Figure 15: Simulation time for different configurations of the reference load case. Superscripts refer to: *a*) smooth T-junction, Figure A.2a; *b*) sharp T-junction, Figure A.2b; *c*) refined radius cf. Figure 14 [Solid 1 mm, refined].

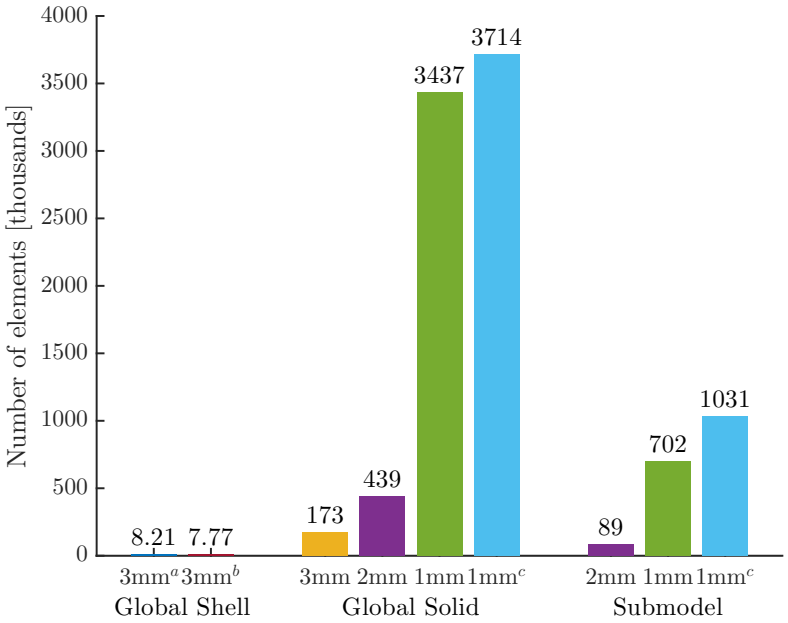

Figure 16: Number of elements for different configurations of the reference load case. Superscripts refer to: *a*) smooth T-junction, Figure A.2a; *b*) sharp T-junction, Figure A.2b; *c*) refined radius cf. Figure 14 [Solid 1 mm, refined].

4.1.2 Response differences

Using different mesh and modelling types, e.g. shells contra solids or global modelling contra submodelling, cause differences in response. To evaluate these differences the first principal strain response is compared between the models. The shell models strain response are compared toward the surface strain response in the global models.

4.1.2.1 Shell and solid comparison

Figure 17 and Figure 18 illustrate the difference in predicted strain levels at two different locations of the model. Point 1 and Point 2 corresponds to the position for the most critical strain levels in the shell and solid models respectively. As seen in Figure 14, these critical points are located in two different areas, i.e. a new hot-spot (Point 2), not found in the global shell model is identified by solid modelling. In the solid models the critical hot-spot is located directly at the radius but in the shell models it is located some distance away from the radius root.

For Point 1, the strain levels are almost identical and differs only within a few percent between the models, see Figure 17 and Appendix C. Modelling with shell elements therefore works well if this area is the part intended to be analysed.

At the radius, for Point 2, the strain response differ more, up to 130% between the global shell and solid models, Figure 18. This is explained by the low mesh resolution in the shell models which does not allow for a correct representation of the geometry at the radius. Furthermore, the shell casting techniques introduce

additional material at the radius, Figure 19. Another effect of this is that the most critical strain levels in the solid models, Point 2, were up to 60% higher than the critical strain in the shell models, Point 1. Consequently, the shell models result in a underestimation of the critical strains in the component, both in terms of location and absolute value.

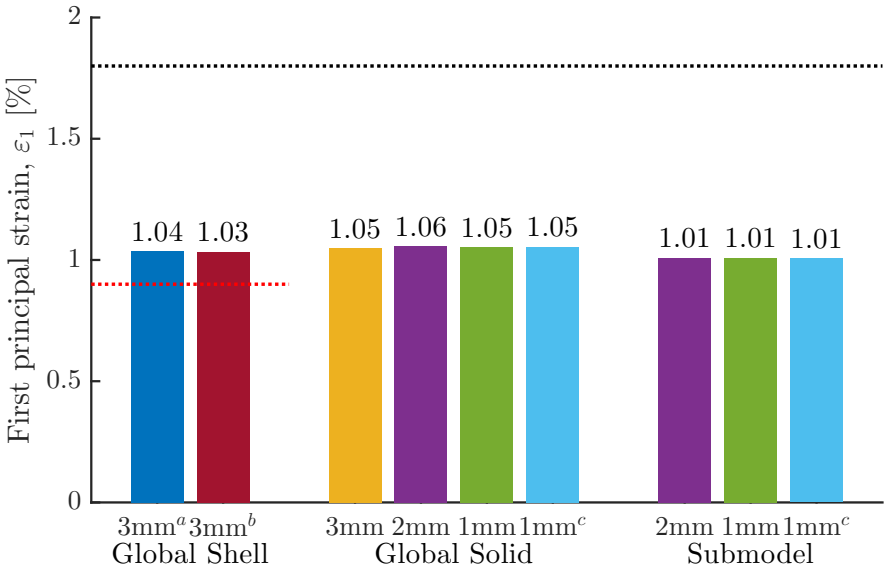

Figure 17: First principal strain response in Point 1 (Figure 14) for different mesh and models. Dotted line: design allowable. Superscripts refer to: *a*) smooth T-junction, Figure A.2a; *b*) sharp T-junction, Figure A.2b; *c*) refined radius.

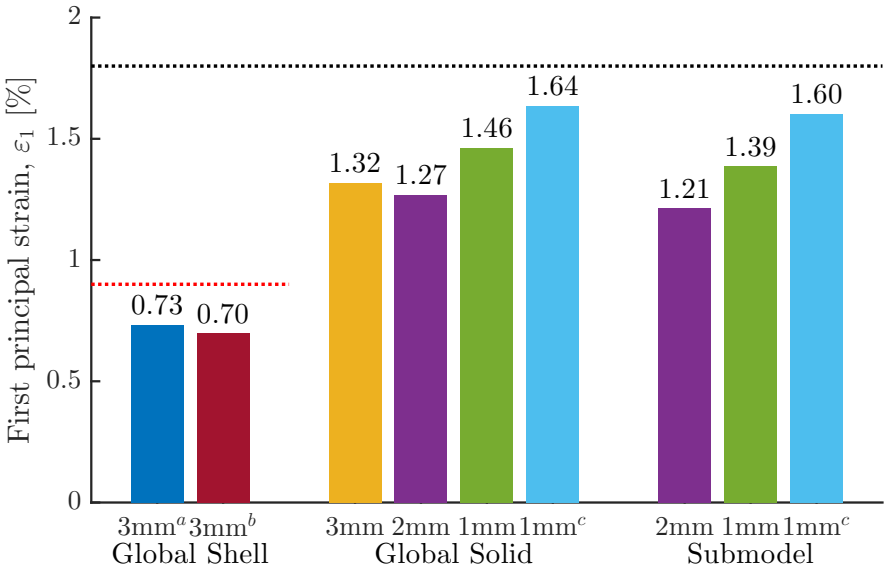

Figure 18: First principal strain response in Point 2 (Figure 14) for different mesh and models. Dotted line: design allowable. Superscripts refer to: *a*) smooth T-junction, Figure A.2a; *b*) sharp T-junction, Figure A.2b; *c*) refined radius.

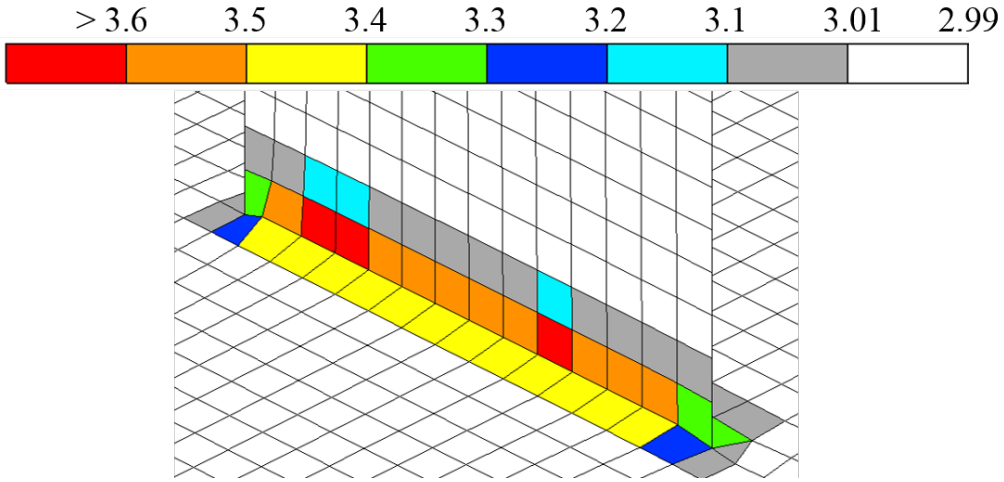

Figure 19: Shell thickness [mm] at radius for the global shell model. Elements in white have a thickness of 3 mm.

4.1.2.2 Global and local comparison

Comparing the strain level response in the global solid models to those in the sub-models with the corresponding element size the differences are small and the sub-model response follows the global solid references well, see bars of matching colour in Figure 17 and Figure 18. In general the submodels predict smaller strain levels than the global solid models, with a relative error of approximately 5%, independently of the considered mesh. As the submodels have prescribed boundary conditions from the global shell model (also with lower response) this can have resulted in that the prescribed values not are exact. However, using full output precision compared to standard (single) precision for the global shell results used to drive the submodels only showed a negligible effect on the response. Details on the output precision are found in Appendix D.1. Onwards full output precision always is used.

4.1.2.3 Mesh dependency

An effect of mesh dependency is distinguished for the strains in the radius, see Figure 18. When the element size is reduced the strain levels increases. With a solid element mesh of 2 mm or coarser there is a problem in dissolving the high strain response in the radius, causing large differences between adjacent elements, see Figure 14 [Solid 2 mm]. With 1 mm elements overall and further refinement in the notch region the mesh allows to capture the high strains caused by bending.

4.1.3 Design evaluation

A strain based design criterion is used allowing for a maximum of 1.8% first principal strain for the specified loading and material [4]. This strain level is illustrated as a black dotted line in Figure 17 and Figure 18. From this follows that all model configurations fulfil the design criterion.

Following the restrictions with a 50% reduced design strain level when evaluating configurations with shell elements in radii (red dotted line), as described in Sec-

tion 2.2, the design evaluation could have resulted differently. If Point 1, which lies on a distance approximately 10 mm above the notch, is included in the restricted area and judged by the reduced criterion the shell models predict strains exceding 0.9%, and hence the design criteria would be classified as NOK. However, as the shell response in Point 1 correlates well with the solid response the most correct way would be to, even here, use the true criterion, i.e. consider that the hot-spot is at sufficient distance from the radius. Consequently, with this approach the shell models also will be evaluated as OK.

4.1.4 Submodel size and boundary effects

In Figure 20 two submodels of different size are compared. The 30 mm model (left) has been cut through the highest loaded region, the radius, while the cut boundaries for the 75 mm model (right) are well away from this region. The overall responses predicted by the models are similar but the maximum principal strain level differs considerably. In the 30 mm submodel the predicted maximum strain is 2.21%, almost twice as high as predicted in the larger submodel.

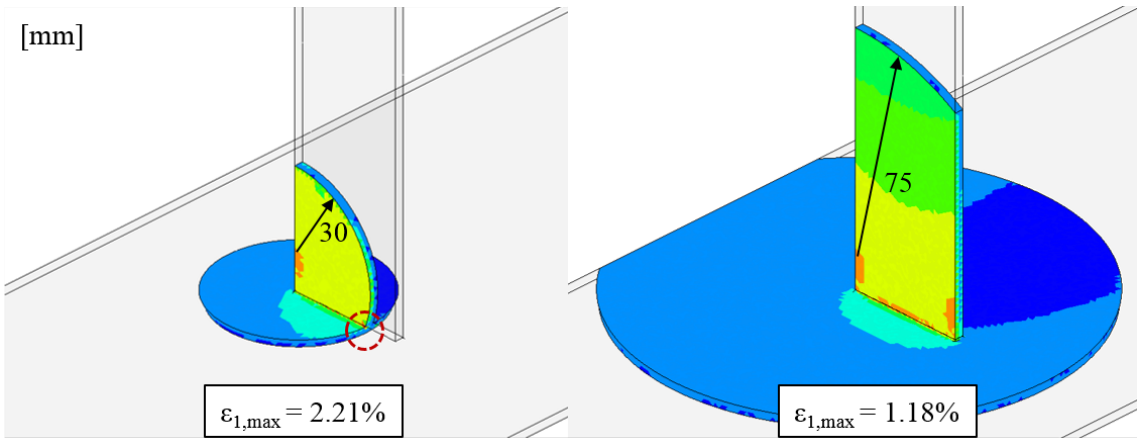

Figure 20: First principal strain response for two different submodel sizes. Left: 30 mm radius. Right: 75 mm radius.

This is a general result also when considering models of other size. Figure 21 presents an overview of the relative error[5] in maximum first principal strain for varying submodel size. For smaller submodels with a radius below 40 mm, the same as the width of the rib, the error is considerably higher then for models larger than 40 mm. The singular elements are always found at the cut interface within the notch, see e.g. encircled element in Figure 20. Excluding the boundary elements result this phenomenon can be fully eliminated, see the dotted line in Figure 21. Besides that the submodel boundary result must be considered with caution this indicates that the attenuation length should be large enough so that it includes the whole hot-spot region. The required submodel size is analysed further for other geometries in Section 4.2.3.2.

[5]Compared to the global solid reference model with similar mesh (2 mm elements).

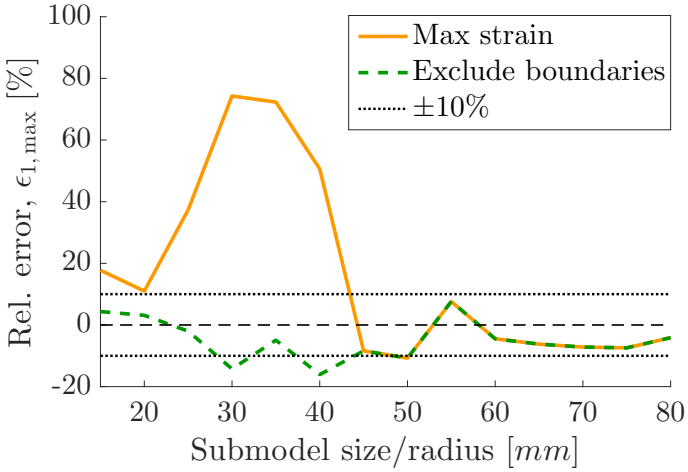

Figure 21: Relative error in first principal strain compared to the global solid reference model with 2 mm element size.

4.2 Trunk lid sillmoulding

The second case study covers a trunk lid sillmoulding, described in Appendix A.2, for which a similar analysis has been done to evaluate consequences of submodelling for a more complex case. This involves more geometrical difficulties and considers not only internal hot-spots but also critical areas located at the interface to other parts. Considering the main requirement for the component, that the principal strain may not exceed the design strain allowable, five critical locations are identified in the global model, see Figure 22. Four of these, marked red in the figure, do not fulfil the material design strain ($>3\%$ first principal strain) while the fifth (E) is marked for further investigation as the strain level in a location close to a radius exceeds the 50% reduced criterion (i.e. 1.5%) used for shell models.

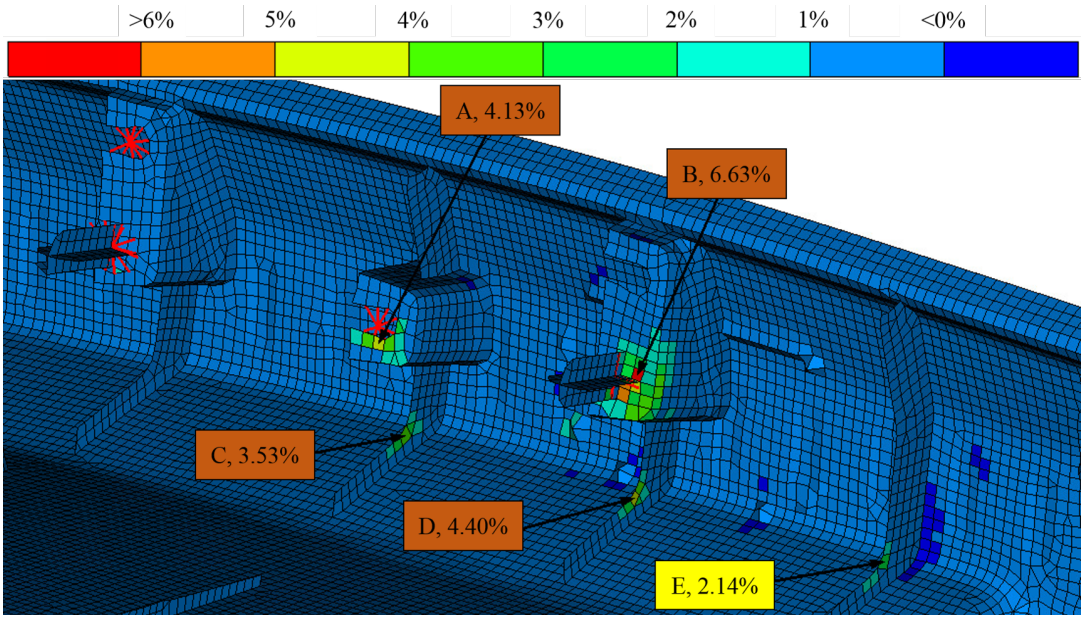

Figure 22: Critical locations in the global model. A-D (red) above design allowable, E (yellow) above 50% of design allowable. Coupling constraints in red.

4.2.1 Submodel responses

For each of the five identified hot-spots in Figure 22 local submodels are created, only taking the trunk lid sillmoulding into account. The submodels are cut as spheres with radius 20 mm and initially modelled with 2 mm solid elements. Figure 23 shows all the submodels created based on location A to E in Figure 22. When comparing the maximum first principal strain for the global and local models, large differences are identified. All submodels, with the exception of Model A, predict a higher maximum strain level at the critical locations. Overall the global shell model only predicted approximately 50-60% of the strain levels in the solid models, see Table 2. Hence, also Model E was evaluated as NOK according to the design criterion.

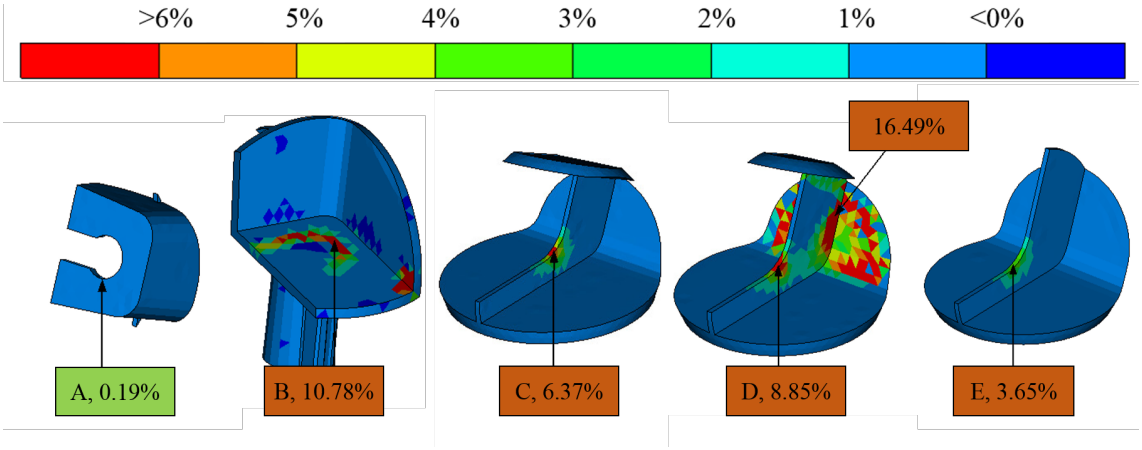

Figure 23: Five submodels (A-E) corresponding to the critical locations in the global shell model.

Table 2: Maximum first principal strain response in the hot-spot regions (A-E).

Model	Strain, $\varepsilon_{1,\max}$ [%]		Ratio
	Global	Submodel	Global/Submodel
A	4,13	0,19	21,74
B	6,63	10,78	0,62
C	3,53	6,37	0,55
D	4,40	8,85	0,50
E	2,14	3,65	0,59
A*	4,13	7,10	0,58
D*	4,40	6,98	0.63

The strain level around the hole for Model A is drastically reduced. This is an effect of only treating the trunk lid sillmoulding and only imposing boundary conditions on the submodel cut interfaces, i.e. the interference with other parts is missed and the submodel response is not representative for the actual load case. In the case of connections and joints further consideration is needed in the submodelling, see Section 4.2.2 for more details. If the connection is included the maximum predicted strain level for hot-spot A is 7.10% (A* in Table 2).

Furthermore, Model D in Figure 23 illustrates the importance of properly imposed boundary condition on the submodel. The rear surface in Model D shows suspicious results with varying strains, even though if this model geometrically is similar to both Model C and Model E without such behaviour. The FE-solver has problems in applying correct boundary conditions to the submodel boundaries due to contact between the trunk lid sillmoulding and the specimen used for applying the load in the global analysis. By excluding the loading specimen from the set of parts in the global model used to drive the submodels this behaviour could be avoided, causing the maximum critical strain level in the hot-spot to drop to 6.98% (D* in Table 2). A more detailed explanation of this phenomena is given in Appendix D.4.

4.2.2 Coupling constraints

Some hot-spots in the trunk lid load case contain couplings to other parts of the car body, see hot-spots A and B in Figure 22. At hot-spot A, in the global model, the coupling was modelled with rigid element constraints between the hole and the car body, representing a clip. A similar representation, using rigid elements, was also used at hot-spot B.

In Figure 24 a submodel with 40 mm radius has been created containing both hot-spot A and hot-spot C. As the submodel is created from the sillmoulding geometry only, information about connections and contacts to other parts is lost. Consequently, at hot-spot A in the submodel, strain levels are negligible due to the absent coupling constraint. However, the strain response around hot-spot C also differs compare to the result from Section 4.2.1, where a smaller submodel was built around this location. This means that the loss of stiffness for this area, due to absence of the coupling constraint, is relatively high.

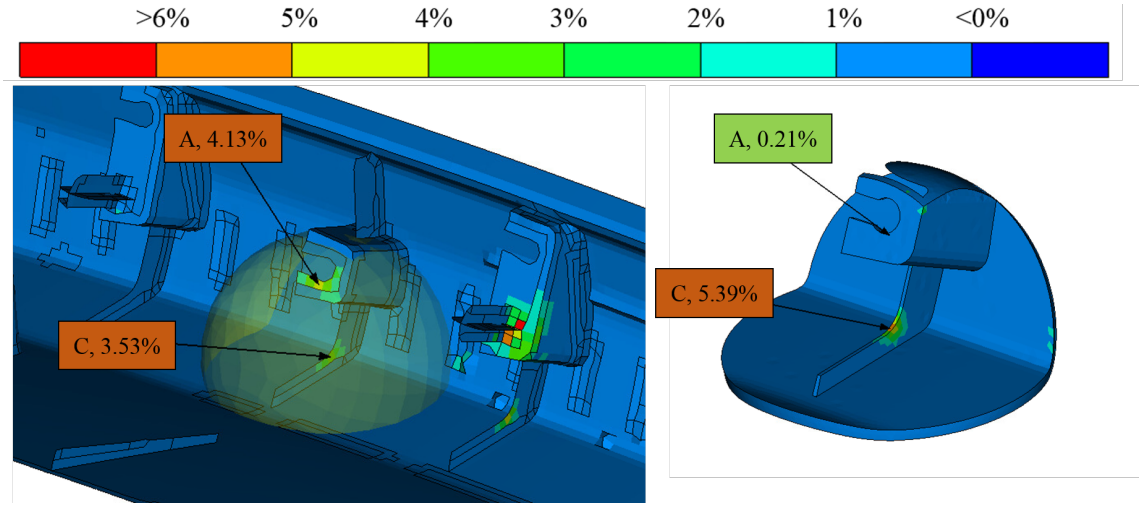

Figure 24: First principal strain for global model and submodel of point A and C.

In Table 3 a comparison between three different coupling configurations is presented. The first configuration, Config 1 is modelled in the same way as the model in Figure 24, meaning that only the intersected faces on the sillmoulding were chosen as

driven boundaries. In the second configuration, Config 2, left in Figure 25, the geometry of the connected car body part is imported and the constraint re-assembled in the same way as in the global model, using rigid body elements. The third configuration, Config 3 seen to the right in Figure 25, is modelled by including the elements at the clip hole to the driven set in addition to the intersecting faces of the sillmoulding. Config 2 and Config 3 can be compared to Figure 12. All three models are modelled with 2 mm solid elements. Both Config 2 and Config 3 captures the global model behaviour in a better way than Config 1 with a strain response ratio more similar to the other models (Model B-E) in Table 2. However, the approach of extending the number of nodes in the driven node set, Config 3 is less demanding to model compared to importing more components and recreate the coupling. Consequently, the computational cost is also reduced. Finally, Config 3 show more conservative results, with the highest predicted strain levels of the three configurations, 79% higher than the global shell model.

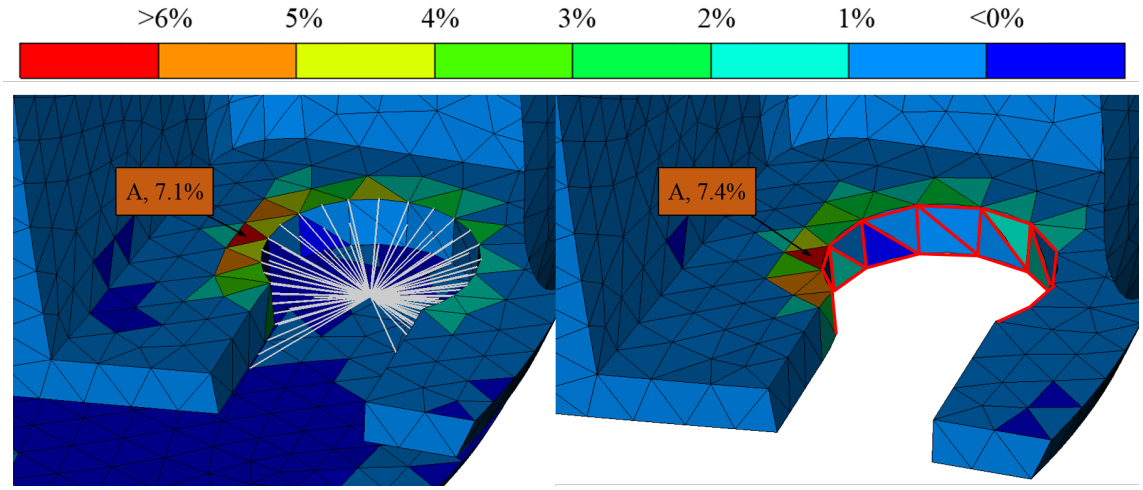

Figure 25: Alternatives on how to handle couplings in relation to the submodel. Left: Config 2, coupling constraints (marked grey). Right: Config 3, driven elements (marked red) at clip hole.

Table 3: Comparison of strain response between different alternatives on how to model couplings inside the submodel.

Model	Description	Hot-spot A		Hot-spot C	
		$\varepsilon_{1,\max}$	Ratio	$\varepsilon_{1,\max}$	Ratio
Global		4.13%	-	3.53%	-
Config 1	Without coupling at A	0.21%	19.67	5.39%	0.65
Config 2	Include connected part and reproduce the coupling	7.10%	0.58	4.91%	0,72
Config 3	Introducing driven nodes where the coupling is connected	7.40%	0.56	4.96%	0.71

4.2.3 Choice of mesh and submodel size

For an efficient method the aim is to create as small submodels as possible without affecting the accuracy in the response by violating St. Venant's principle. As the assay volume is reduced, by creating local models, this may enable use of even finer mesh configurations to further improve the accuracy in the analysis. Therefore, a converged solution where both the mesh and the submodel size are taken into consideration is needed. Below studies of variations in both element size and submodel size in the trunk lid sillmoulding load case are presented.

4.2.3.1 Varying element size

Previously 2 mm solid elements were used for submodelling the sillmoulding. This was according to the recommendation for solid element models in the VCC guidelines [2]. To further analyse a suitable element size for the submodels, which also was done for the reference load case (Section 4.1), different meshes are tested in the submodelling process. Model A and E (Figure 23) are chosen as these differs geometrically and are exposed to different load types. In Model E the critical areas are loaded in pure tension/compression and in Model A also bending is introduced through the clip. The models where cut at a distance 20 mm and 30 mm for Model A and E respectively. The coupling in Model A was modelled using the approach by adding driven nodes at the hole, cf. Config 3 in Table 3.

Figure 26 shows the submodel response at hot-spot E using two different element sizes, 2 mm respectively 1 mm elements. Further refinement was also studied as presented in Appendix D.2. Due to pure tension loads acting on the hot-spot, the response patterns are almost identical. Consequently, the change in predicted maximum strain ($\approx 3.8\%$) in the hot-spot was also small, Table D.2. A mesh with higher resolution affected the simulation time only which was drastically increased as the mesh was refined, Table D.2.

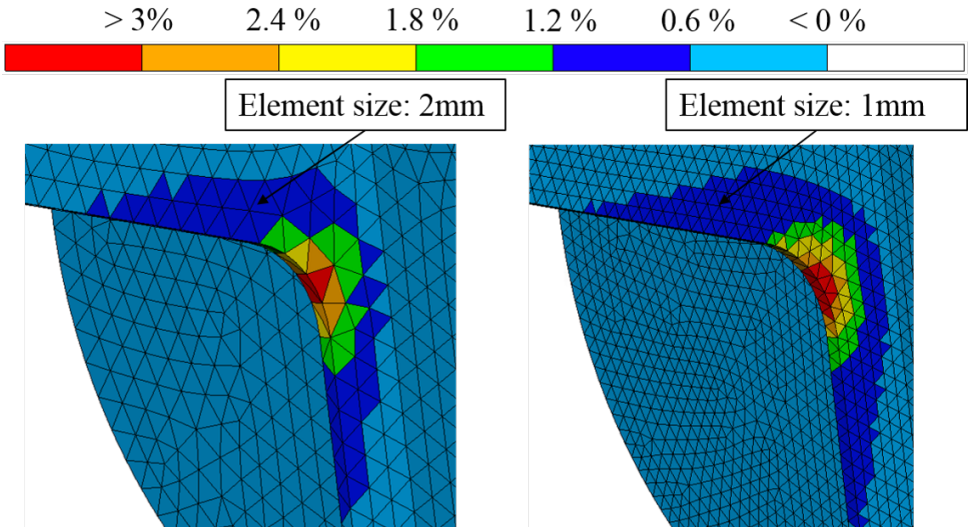

Figure 26: First principal strain response patterns at hot-spot E using two different element sizes.

Variation of the mesh size for Model A shows larger differences in strain response. A finer mesh significantly improves the resolution of the geometrical details and the strain response distribution, Figure 27. Furthermore, as noticed before, the coupling in the model causes large strain levels in the elements at the hole which are connected to the rigid elements. When reducing the mesh element size this effect is still conspicuous, even though it becomes more concentrated, i.e. a smaller area and higher maximum strains, see Figure 27 and Table D.1. This is an effect of modelling the coupling with rigid elements, as the stresses in elements at the hole edge connected to the rigid elements becomes singular.

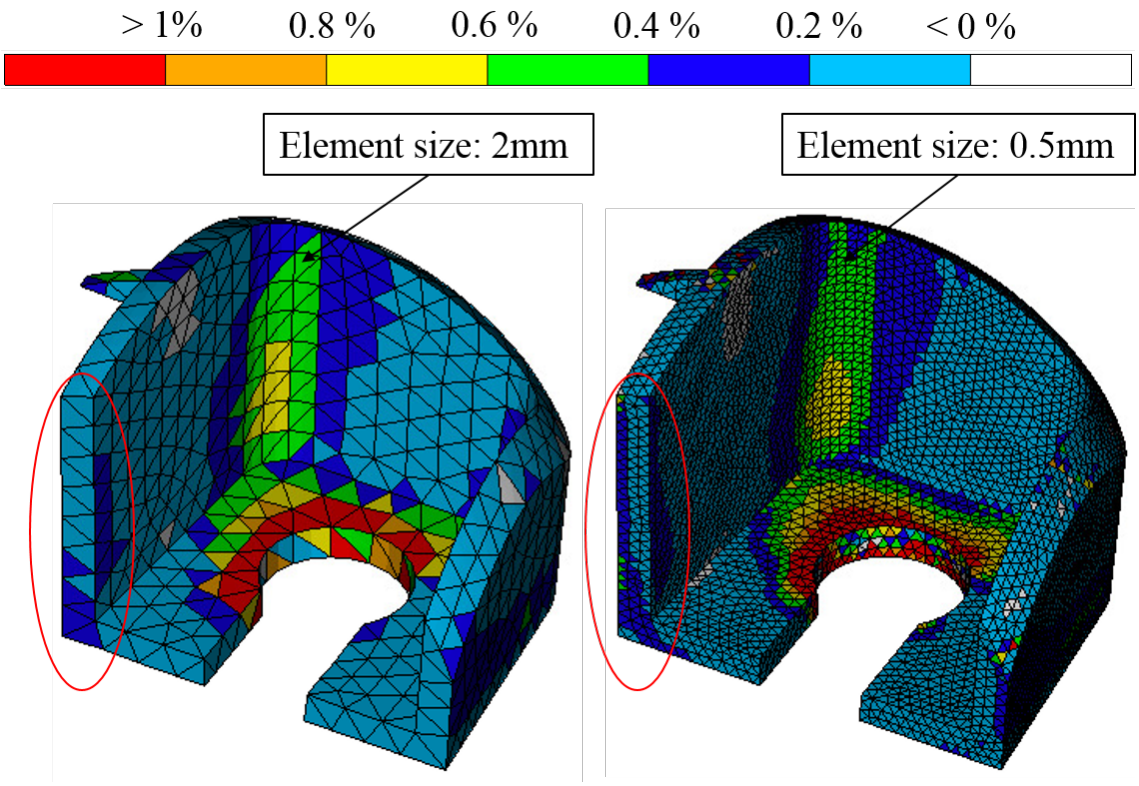

Figure 27: First principal strain response patterns for Model A using two different element sizes.

Moreover, the existence of the coupling cause bending deformations at the surrounding edges of the submodel when applying the load, e.g. in the encircled area in Figure 27. In this area the mesh of 2 mm elements (one element across the thickness) is not enough to capture all bending effects as shown. Using 1 mm or 0.5 mm elements resulted in between 1.4 to 3 times higher strain levels over the thickness in this area compared to the original 2 mm mesh.

Therefore it is recommended to use an element size that allows for having at least 2-3 elements over the thickness in presence of bending loads. In this case, 1.0 mm elements are on the limit of what is considered sufficient. With the submodel volume size with a radius of 20 mm the simulations using the most refined mesh, 0.5 mm was solved in approximately 3.5 minutes, for more details see Appendix D.2.

4.2.3.2 Varying submodel size

For both Model A and Model E the volume size of the submodel was varied while the mesh was held constant using 1 mm elements. A smaller submodel volume size causes the driven boundaries, where the strain response may become inaccurate, to come closer to the analysed hot-spot. Excluding result from the driven boundary the maximum first principal strain response for Model E is given in Table D.3 and visualised for models with radius 18 mm and 5 mm in Figure 28. The overall strain response is similar for all models. Only when considering the smallest volumes with sphere radii 5 and 8 mm, the relative error of the maximum critical strain starts to diverge, see Figure 29b and Table D.3. For these models the strain gradient is considered to be to high in the area where the models were cut. However, such small models would in this case probably not be of interest as the total geometric characteristic, i.e. the radius where the hot-spot is found, is larger than the submodel itself and e.g. design optimisation in a later step would not be possible. The model must of course always be larger than the area that is analysed. Furthermore, as the submodel volume becomes small even finer meshes can be used without a significant affect on the simulation time.

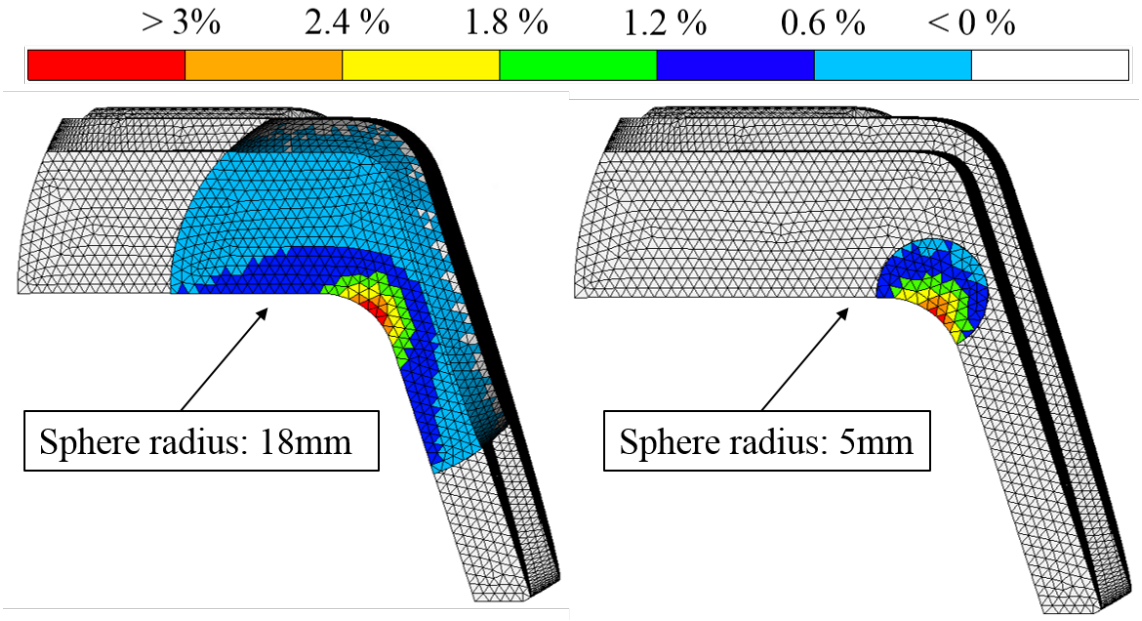

Figure 28: First principal strain response patterns at hot-spot E for two different submodel sizes. Largest submodel (32 mm) used as reference in transparent.

For Model A the relative error in predicted maximum strain was not as distinct as for Model E, Figure 29a or Table D.4. Also, the overall response pattern was not the same for all models. A smaller model, exemplified by a radius of 5 mm in Figure 30, shows significantly higher strain response values. In this case the couplings around the hole is believed to have a large influence and cause the large strain variation when the total model is smaller. For a stabilised response a model of radius 18 mm or larger was found necessary. The strain response of the 18 mm model in Figure 30 is consistent with the response in Figure 27, so is the relative error presented in Figure 29a, which is small.

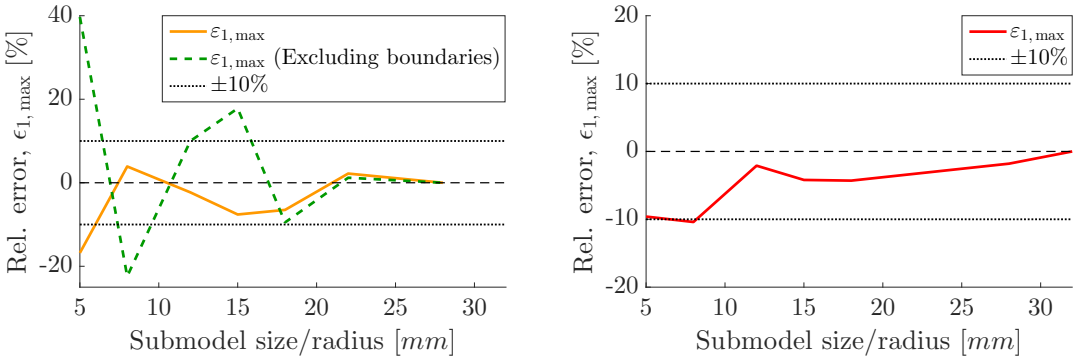

(a) Hot-spot A **(b)** Hot-spot E

Figure 29: Relative error in maximum first principal strain compared to the largest submodel for each hot-spot.

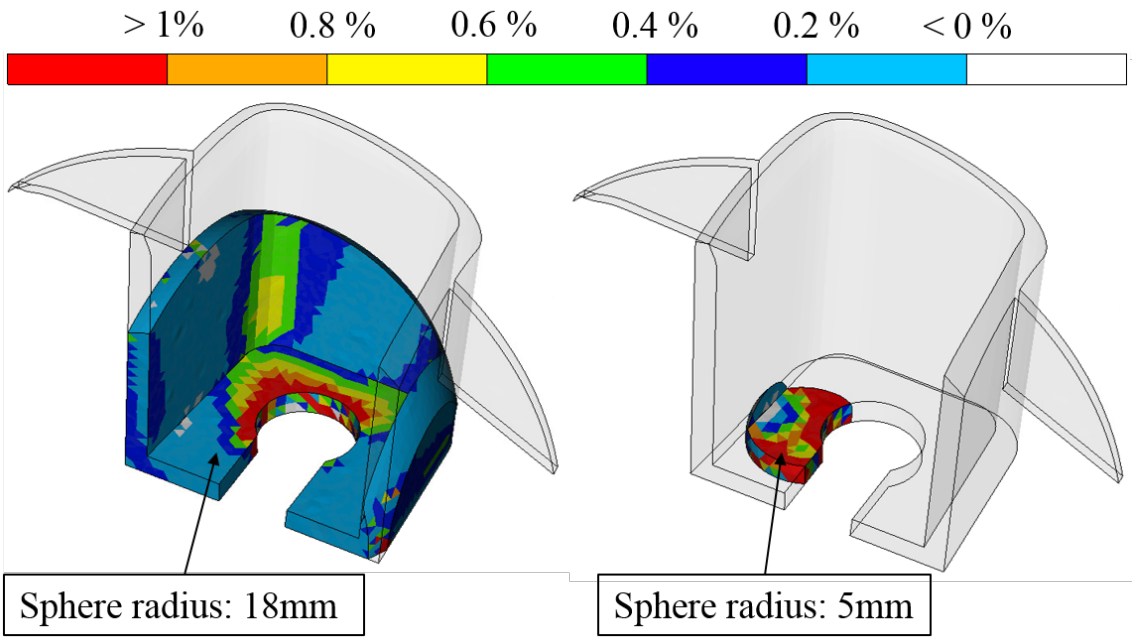

Figure 30: First principal strain response patterns at hot-spot A for two different submodel sizes. Largest submodel (28 mm) used as reference in transparent.

5 Correlation

To validate the efficiency and accuracy of the submodelling approach the predicted strain levels of the submodels are compared to the measured strains on a physically tested component. Similarly, the global model's strain response is compared to better understand the improvements by the local modelling. The analysed load case, rear door sillmoulding, is used to verify the strength and stiffness of the sillmoulding. For more details about the load case and test setup see Appendix A.3. Normally, the correlation parameters are the force and displacement which are measured at the loading position and compared to the FE-simulations. However, the aim of submodelling is to evaluate hot-spots, not necessarily appearing at the loading position. Simultaneously, the submodel displacements are partly prescribed from the global model. Thus, the improvements by comparing the submodel displacement to the test instead of the global model response, become hard to distinguish. Below the correlation is focused on comparing FE-responses in relation to the identified defects in the test, see Figure 31, both regarding size and intensity in the area.

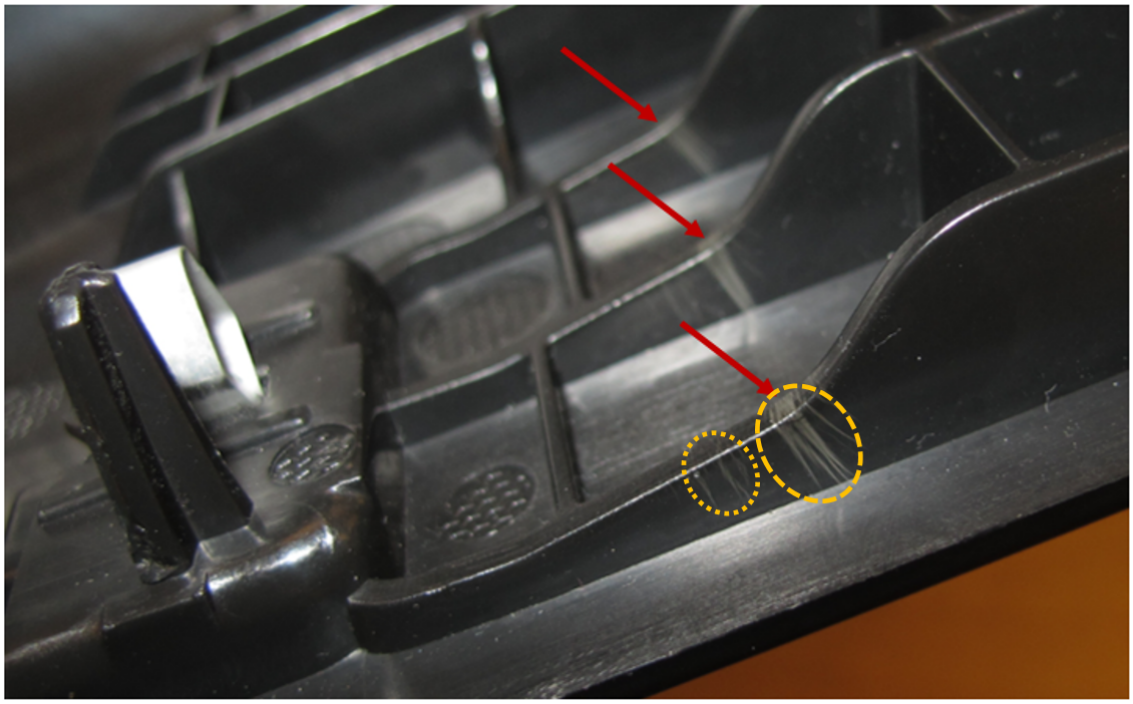

Figure 31: White marks (crazing) in T-ribs under the rear door sillmoulding.

In the test three critical locations with crazing defects were detected as shown in Figure 31. By using the submodelling approach in Section 3 the same hot-spots were also identified in the global FE-model. The hot-spots were located at the ribs under the load device and have their maximum strain levels in the radii. For the submodel volumes spheres with radius 20 mm were used. However, as the strain levels of the global model were widely spread, see Figure 32, the three submodels were merged into one subvolume domain. The submodel was meshed with 1 mm elements according to the outcome of the convergence study in Section 4.2.3.1.

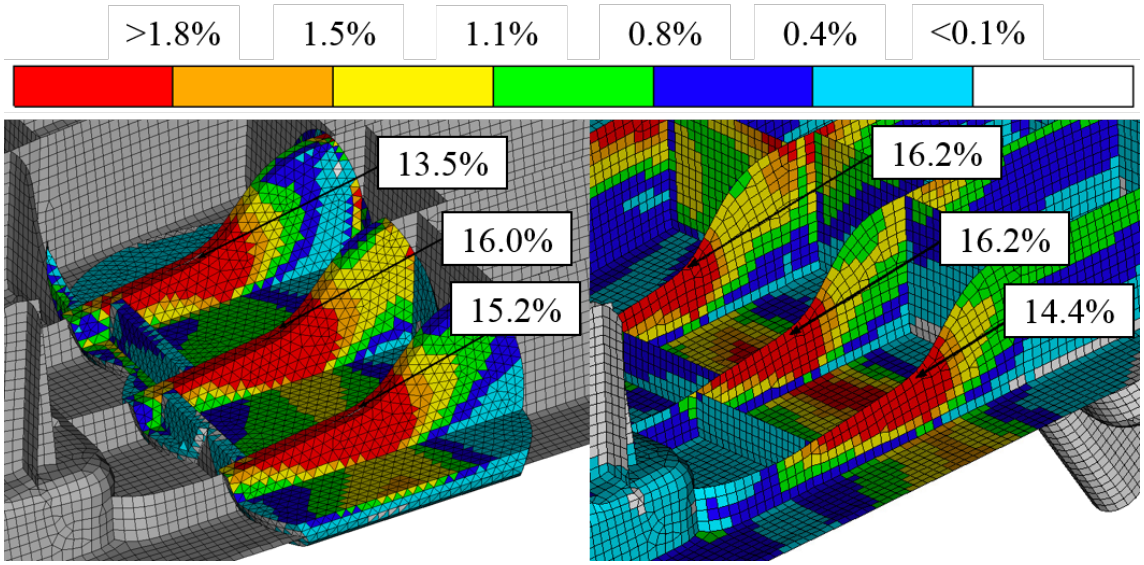

Figure 32: Elements exceeding the design strain (1.8%) marked red. Left: Submodel. Right: Global model. Annotations for the maximum strain level for each ribbon. [First principal strain, %].

The areas of the white marks in Figure 31 can easily be observed in Figure 32 where the strain levels for both the global and submodel have exceeded the design allowable (1.8%). Unlike for previous analyses made in this project the maximum strain levels at the three ribs are similar between the global shell model and the solid submodel. The global and local models differ more when comparing responses in the areas between the ribs. In these areas the shell model generally predicts higher strains which exceed the design allowable. However, in the test, no evidence on damage in these areas could be identified, which indicates that the submodel response is in better correlation with the test response.

The elements predicted to sustain strains that exceed a yield strain of 2.6% are plotted red in Figure 33. These patterns, of the elements exceeding the yield limit, correlates well to those of the white marks in Figure 31. However, in case of the submodel, this also predicts crazing in the smaller area, left circle in Figure 31, more accurately and to a higher extent.

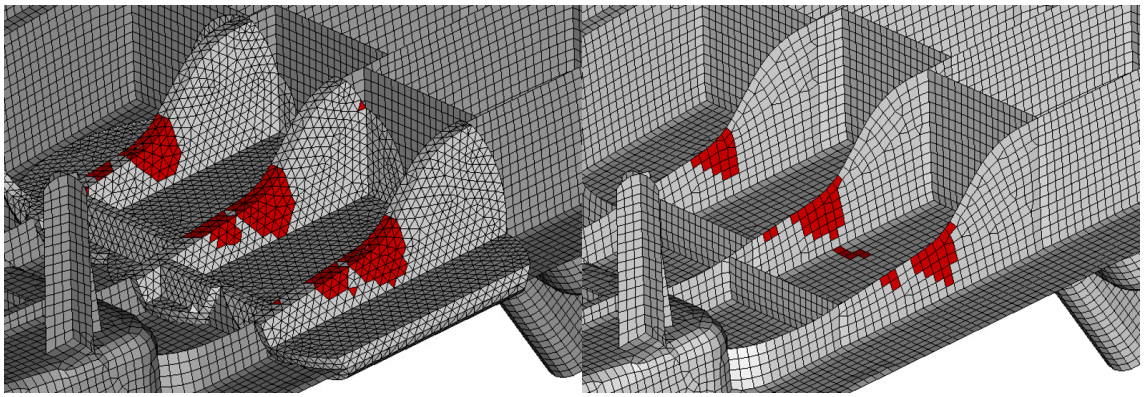

Figure 33: Elements exceeding the yield strain (2.6%) marked red. Left: Submodel. Right: Global model [First principal strain %].

6 Scripting and automation

To simplify the modelling and make the submodelling approach user-friendly, Python scripts to perform the modelling steps in Section 3 are developed. Instead of a "black-box" solution, the scripting was aimed to allow the user to interact with the modelling process. The link, between the user and process steps, is done by creating Graphical User Interfaces, GUIs, where the user is given control and feedback on the submodelling.

Overall, the script is divided into three main modules, which are independent of each other: One script for post-processing the global model; one script to pre-process and model the submodels; and one script for post-processing the submodels and to compare the results to those from the global model. The functionality of the modules were verified by utilising the scripts for the load cases described in Appendix A and compare the outcome to the result in Section 4.

6.1 Post-process of global model

The script for handling the global model is developed to be used in the post-processor. Thus, this implies that the global model must already have been created and solved before the module can be utilised. The main purpose of the script is to assist the user in analysing the global response and to define the parts to be submodelled. Figure 34 illustrates the main steps where the script can support the user in white boxes. The input and output for each step are given in the upper and lower boxes in Figure 34, respectively. From a specified design criterion and threshold value hot-spots are easily identified and the submodel volumes are defined around them. In Figure 35 an overview of the corresponding GUI for this procedure is shown.

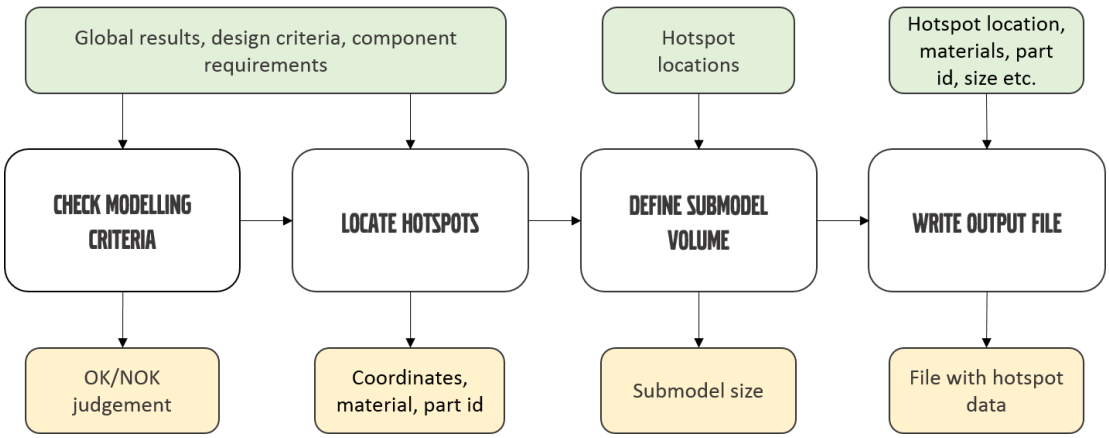

Figure 34: Main parts in the global post-processing script.

In the following description the encircled markers refer to the matching markers within Figure 35. As the script was developed to connect with the current Meta session the user may chose only to make use of parts of the GUI, e.g. if some critical points have already been located in a current model the user may use these to define the submodels instead of loading a new model or defining any modelling criterion.

At the top of the window the user is asked to specify the geometry file ① and the result file ② for the global model in which the submodels shall be defined. If a model already is loaded in Meta these fields are automatically filled. It is recommended that the Abaqus input file (*.inp*) is used for the geometry. This recommendation is given to include information about all couplings and constrains and to ensure that the correct materials and part names are loaded. Nevertheless, the output file (*.odb*) may be used for both geometry and results.

Depending on the active result file, the scalar list window ③ updates with all available scalar functions for the model. Singular elements, due to rigid connection elements, loads, etc., can be excluded by ticking the *"Exclude Singularities"* box (4a). If the result of interest is not already loaded the user has the option to do so by ticking the corresponding box and press the load button (4b).

In the scalar list window ③ the user has the opportunity to specify a criterion for the available scalar result. To do this the user must activate the criterion by ticking the criterion box and specify the design condition ⑤. This could be e.g. " > 0.015" which means that regions with response values above 0.015 shall be identified.

The lower part of the GUI is used for identifying the hot-spots and defining the submodel volume in the active model ⑥. The active model is automatically changed if new results are loaded. This is only needed if the user has several different models loaded in the active window of Meta. For identifying hot-spots two options are available. Either the script uses elements that already have been predefined as hot-spots by the user (7a) or the previously defined design criterion is used (7b). The critical locations that are found are displayed in the submodel list window ⑧. Here information about the hot-spot location, it's scalar value and the submodel size etc. are given. For each hot-spot a submodel volume automatically is defined. In the standard configuration this is a sphere with a radius of 20 mm. If a hot-spot is selected in the list the defined volume is visualised in the Meta window. By changing the volume size in the list the user is directly given feedback on how the submodel size relates to the total model geometry. In such way a sufficiently large submodel can easily be defined. If identified hot-spots are located close to each other and/or lies in geometrically difficult areas it may be hard to find a good representation of the submodel size for each hot-spot. In such case a larger volume can be created by collecting several volumes into one, including all necessary hot-spots. New hot-spots or unwanted models can be manually removed or added to the list (9a).

The user also is informed, via the submodel list window, if connections exist in the defined volume. This to indicates when extra consideration is needed in the submodelling. The connecting parts and their corresponding material ids are outputted in the list.

When the hot-spots have been located and the submodel volumes been specified the information in the submodel list window ⑧ are written to a text file by pressing (9b). The generated file consist of information about the hot-spots locations and the global model analysis definition needed to construct comparable submodels. The file is outputted in the same directory as the geometry file of the global model with the name *global model name_hot_spot.txt*, see example in Appendix B.

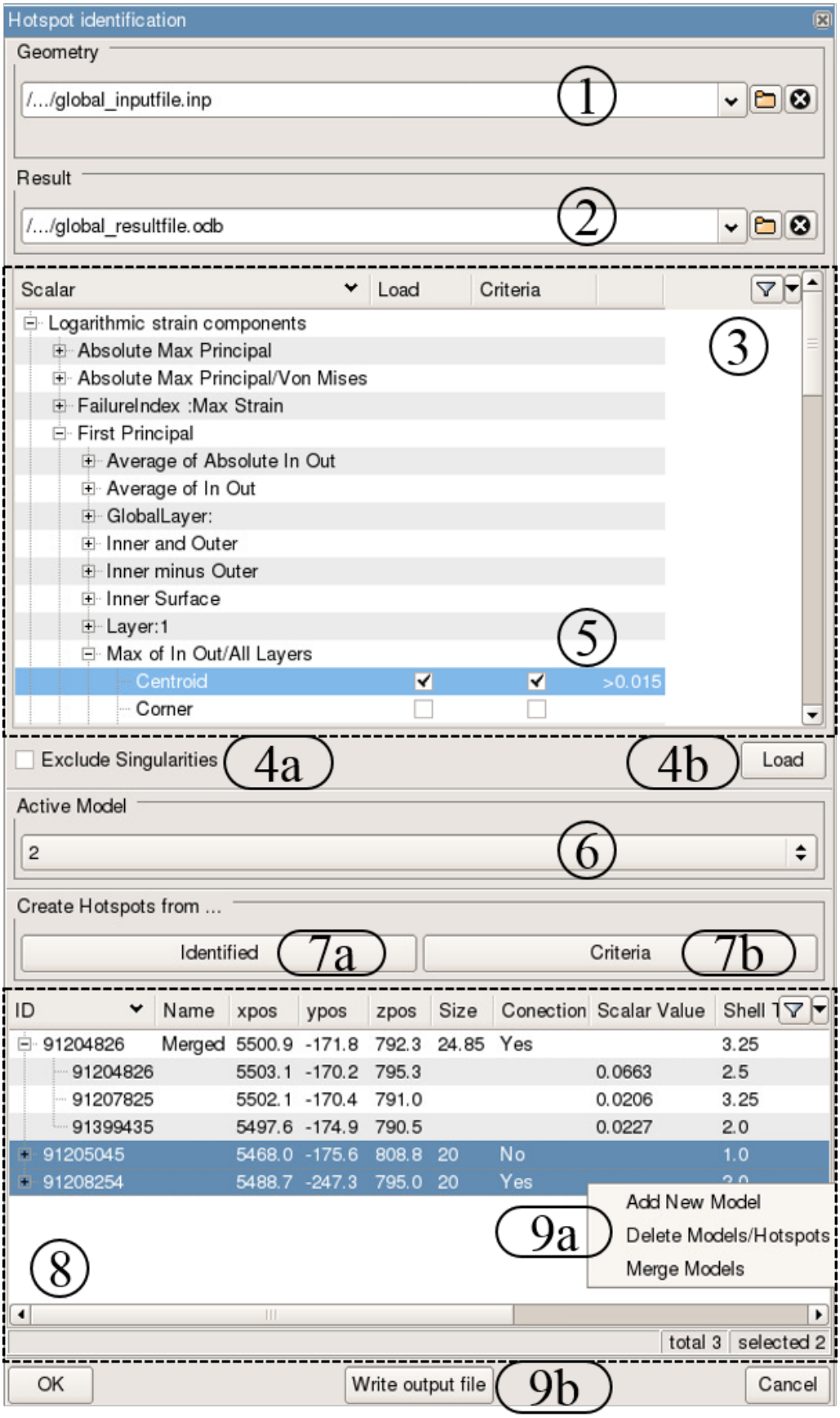

Figure 35: Hot-spot identification GUI for post-processing of the global model.

6.2 Pre-process of submodel

The submodelling is done in the pre-processor Ansa, for which a script is developed. Figure 36 gives a schematic overview of the steps in the pre-process method that can be handled by utilising the script. The step of how to locate and retrieve the correct CAD-files for the parts of which the submodels are to be built is not included in the script. This step must be done manually and the CAD-geometries be given as input to the script. However, if the naming of the components in the global FE-model is done correct, the name corresponding to the CAD-files are output in the hot-spot file as discussed in the post-process step of the global model above.

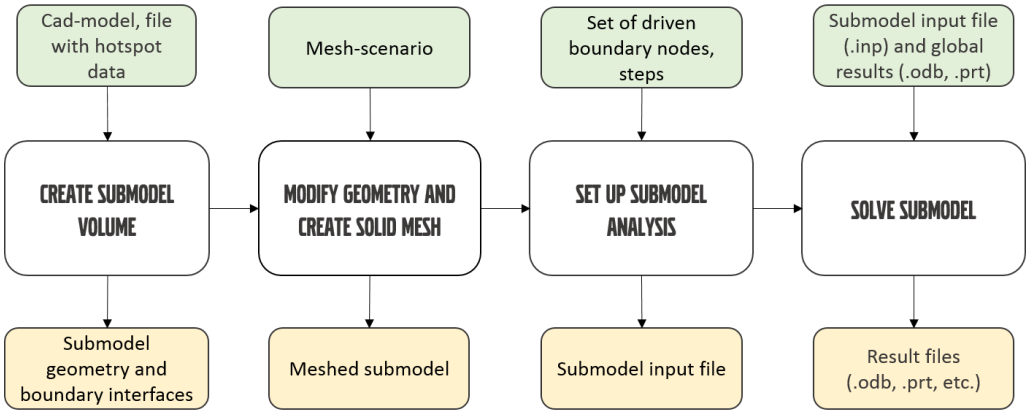

Figure 36: Flow chart for pre-process script.

In addition to the CAD-geometries, information about where to build the submodels is needed. Therefore, the user initially is asked to select the hot-spot file, CAD-file, global solution (*.odb*)-file and the desired work directory, where the submodels should be outputted, see Figure 37. A preview of all submodel volumes as they were defined in the post-processor is given. The user may choose to create new submodel volumes, modify existing ones, merge coinciding volumes to one compound sub-model volume or delete unwanted volumes, see Figure 38. Upon confirmation of the submodel volumes the hot-spot file is updated with the changes accordingly.

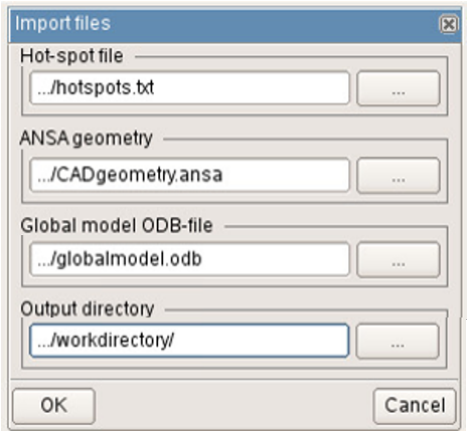

Figure 37: File input GUI.

Figure 38: Modify and confirm submodels.

The script loads the CAD-file and the defined volume for each submodel in the hot-spot file. The volumes are automatically intersected from each other to define the submodel. Also, the interfaces between the full geometry and the submodel volume are saved as a new set ("*Driven_set*") used to drive the submodel analysis. The user is asked to confirm, or possibly add/remove faces from the driven node set. If the volume domain contains couplings or contacts the corresponding surfaces/elements can be added to the driven boundaries, see Section 4.2.2. The driven node set is automatically prescribed as boundary condition, the shell thickness is specified and the correct load steps that refer to the global solution file are created.

The fact that the script is developed as an extension to Ansa, enables the user to take advantage of all functionality already available within the pre-processor. The user may therefore modify the geometry of the submodel, e.g. add missing details such as radii. This is most preferably done after the volumes are intersected to avoid unnecessary work in areas not intended for further analysis. Similarly, the meshing can be done manually using the standard Ansa tools. However, for convenience, some batch mesh scenarios are implemented in the script, Figure 39.

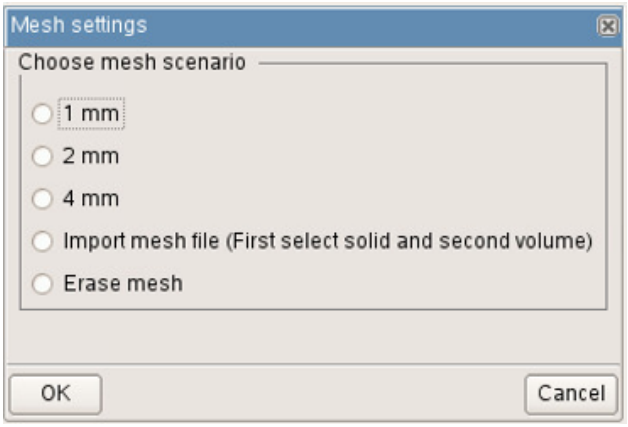

Figure 39: Mesh setup GUI.

The above procedure is repeated for all submodels specified in the hot-spot file. Each submodel analysis input file is exported to the work directory.

6.3 Post-process of submodel

For each global model that is analysed, there could virtually be an unlimited number of associated submodels to evaluate. Already for a low number of submodels it becomes demanding to manage and keep track of all models. In the post-processing step the models must be imported into Meta to be evaluated and compared to the global model response. Furthermore, when only a small part included in the submodel is shown, it becomes difficult to distinguish one submodel from other submodels as well as it's corresponding location in the global model. For this purpose a script to easily import and visualise the response for several models is developed. Together with the hot-spot identification script, Section 6.1, the models can be evaluated towards a design criterion. Figure 40 gives an overview of the main steps in the submodel post-process script.

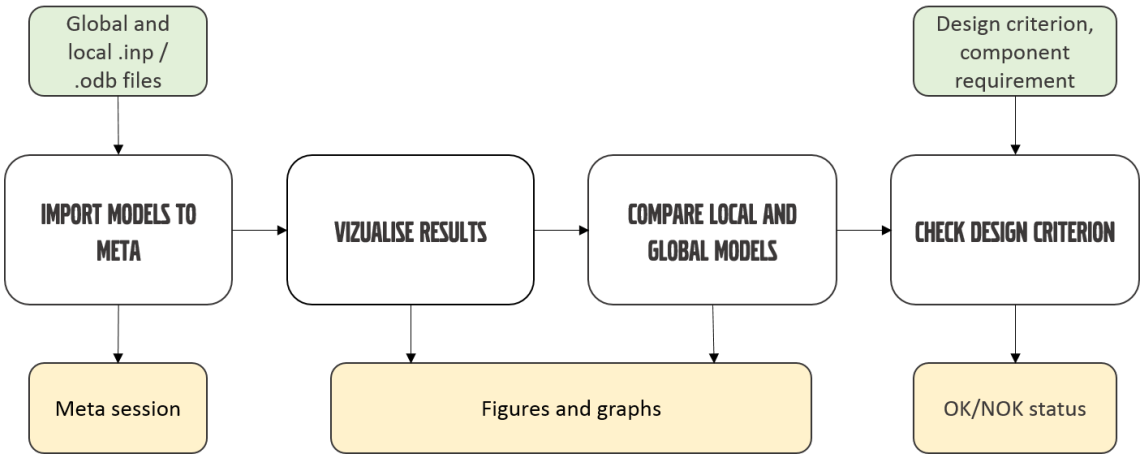

Figure 40: Main parts in the submodel post-processing script.

The inputs to the post-process script are given in input files (*.inp*) and/or result files (*.odb*) for the global and local models respectively. In (10) (Figure 41) several files can be selected at the same time. If the *.odb* file is given this is used for both geometry and result. Alternatively, if the *.inp* file is given as input this is used for the geometry and the script automatically tries to find the corresponding result file. It is also possible to input a text file (*.txt*) containing a list of the file paths. The input information is displayed in (11). The user may select which models that shall be loaded as global and local models respectively.

The most common scalar results are predefined in (12) and can be chosen for visualisation. Before loading it is possible to exclude singular result (require *.inp* file as input). The user may chose if the contour of the global model should be shown together with the submodels (for easier localisation) or if each submodels should be loaded separately (13).

The outcome for the trunk lid model could look as shown in Figure 42. To check the design criterion for a submodel; load the hot-spot identification script, Section 6.1 and change the active model to the id corresponding to the submodel ((6) in Figure 35). The models may then be evaluated as described in Section 6.1.

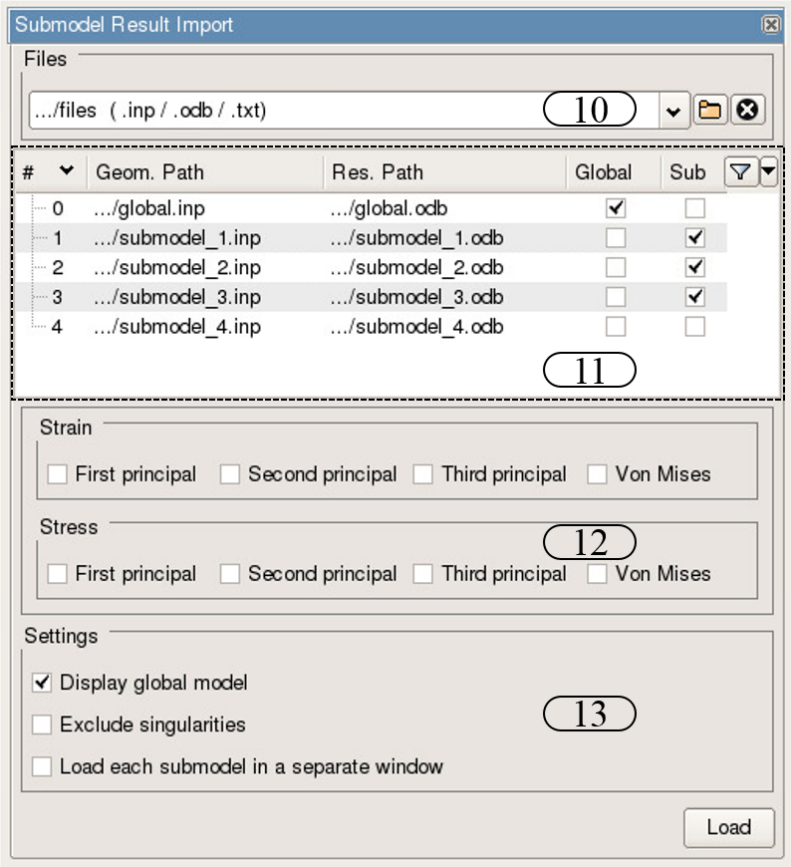

Figure 41: GUI used to import and visualise response from several models simultaneously.

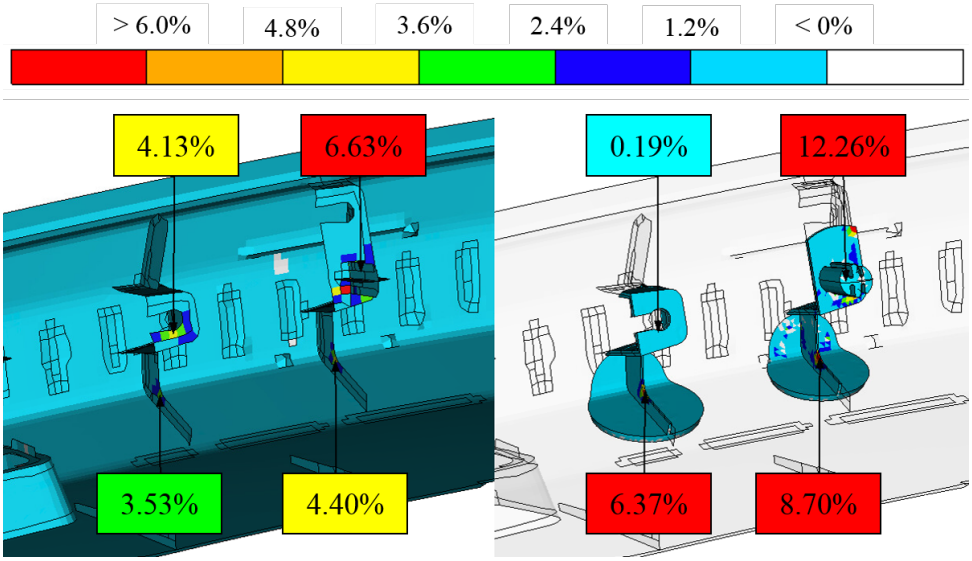

Figure 42: Visualisation of first principal strain response of the global trunk lid model (left) and corresponding submodels (right).

7 Discussion

The purpose of this master's thesis was to create an automated multiscale modelling method to increase the accuracy of FE-analyses while simultaneously keeping lead times short. For this the submodelling technique was used. Considering the reference case, it was proven that by using this approach the aim has been met. The computational cost for the global shell model and the submodel together was only a small fraction compared to the computational cost for modelling the whole component with solid elements, Figure 15. At the same time, the submodel strain response was close to the response predicted by the global solid reference model.

Both in the reference and the trunk lid sillmoulding load case the global shell models generally predicted lower strain levels than the solid submodels. The strain levels in the shell models were 50-60% of the strain levels predicted by the solid models, e.g. see Table 2. This is a consequence of the Ansa shell casting technique together with a low resolution mesh. The extra material affecting the elements in vicinity of such T-junction, see Figure 19, is believed to cause an overly stiff shell solution of the area. A finer global shell mesh resolution may possibly solve this problem, as the thickness error is evened out, but this will have negative effect on the computational cost.

The rear door sillmoulding model showed less differences in maximum strain levels for the global model and submodel. This may have been caused by that the global model of the rear door sill was modelled with a finer mesh resolution compared to the mesh of the trunk lid model. This was possible as the rear door model was a much smaller model, with less components, than the global trunk lid model. Also, the fact that there were no sharp radii at the hot-spots and that the shell elements were loaded in tension, where shell modelling works better, may have influenced the strain response.

Regarding the submodel size it was proved that the submodels often may be taken fairly small. However, due to geometric properties and the size of the stress concentration a general minimum size of the submodel is hard to determine. The needed size varies from case to case, which complicates a fully automatic process as some engineering judgement often is necessary. As a rule of thumb, due to discrepancies at the submodel boundaries, it is better with a too large rather than too small model to minimise the risk that the hot-spot response becomes affected. For smaller components, where the attenuation length is in the order of the component size, it is possible to use the whole component as a submodel with the correct boundary conditions. This eliminates the need of creating a submodel volume.

The recommended element size of 2 mm, according to VCC standards [2], was in some situations not allowing for a fully converged solution. In sharp radii and when bending loads were applied a refined mesh had to be used. However, the use of second order elements is thought to be beneficial and reduce some of these effects.

In this study uniform meshes, with constant element target length, were used when evaluating the submodel response for different element sizes. However, due to that the interpolation of the boundary conditions is made based on only one value in the

2D-mesh, at the middle surface of the geometry, a fine 3D-element mesh with several elements across the thickness at the submodel boundary is unnecessary. A higher mesh resolution is only needed and desired where the hot-spot is located, i.e. in the centre of the submodel. Therefore another meshing approach would be to have varying element size, a coarser mesh at the boundaries and a refined mesh closer to the centre of the submodel. Consequently, this can further reduce simulation times.

In the case where the submodel volume contains coupling constraints the study presented two approaches. Inclusion of couplings, see Figure 25 (left), causes the driven boundaries, where disturbances from the applied boundary conditions may appear, to move further away from the hot-spot. However, due to that the couplings are modelled with rigid elements, causing singularities, it is believed that the strange boundary effects becomes less important when these elements also are used to drive the submodel, see Figure 25 (right). For this reason the use of driven nodes instead of couplings is also a good alternative. In either case, it is not recommended to use these elements for evaluation of the submodel. Alternatively, solid modelled clips can be used. Such an approach will however require additional data for the clip and often increase the computational cost and result in convergence problems due to contact and friction between the bodies.

The submodelling method may always be used to resolve and better predict stress and strain concentrations. However, due to the fact that submodels seldom predict significantly lower response levels this mean that if a global model cannot fulfil the design allowable in a certain area, the corresponding submodel will probably also fail. Hence, in these cases and only for evaluating the design as OK/NOK, the submodelling approach may be unnecessary. In other cases or with the aim to better understand why the concentration appeared and how it can be resolved, submodelling is beneficial. Especially as it enables for design optimisation on a local level.

The analyses made in this study are based on a limited number of geometries, therefore the recommendations of submodel volume and element size cannot be guaranteed to hold for all kinds of geometries and load cases. However, the guidelines stated are assumed to be representative, as several different kinds of geometries and load types have been evaluated.

Even though the script that was developed for the submodelling approach is more or less automatic, the user still needs to be attentive for e.g. contact and coupling constraints that may appear in the models. By automating the submodelling approach, a balance between what parts of the process that should be performed in a black-box operation and what parts should be carried out manually has been made. It is important that the user is observant and uses engineering judgement to evaluate if the model response is accurate enough or if some parts in the modelling process has been missed out.

Using the scripts showed to reduce the time needed for preparation of the submodels. One must still remember that exactly how much time that can be saved is a highly personal dependent parameter and will depend on the number of hot-spots.

8 Future work

In this study, only isotropic materials have been considered and analysed. One of the benefits of using the submodelling approach in this thesis is that it also can be implemented for analysing more complex materials such as composites.

The process described was also chosen to be implementable with the software used at Volvo today. However, it can be interesting to evaluate the differences in computational cost and accuracy of results using different approaches and also using different kinds of geometries than a sphere used in this thesis work. The submodelling procedure implemented in Abaqus uses a distinct submodel transition with shell-to-solid couplings which caused discrepancies in response at the submodel boundaries. In future work it may therefore be beneficial to implement submodelling with a smooth transition and eliminate this effect, e.g. using MST [5][10].

In the future it may also be possible to extend the submodelling approach with new features e.g by implementing looping work, such as design optimisation of the submodel volume domain, and thereby improve the efficiency of the process even more.

9 Concluding remarks

A multiscale modelling analysis framework has been developed using a submodelling technique. The presented submodelling approach provides detailed and accurate FE-results at a low computational cost. Implementing the approach and enable for starting to accept designs in an earlier state instead of first evaluating them as NOK according to the 50% margin factor for shell element models saves both time and money. Furthermore, this means that the properties of each material can be utilised to a greater extent. By modelling components with solid elements and a high resolution mesh the models better represent the true geometry and capture radii and other details that are neglected using shell elements and coarser mesh.

The study shows that by using a sphere as submodel volume the submodels can be as small as 20 mm in radius with converged results of sufficient accuracy. For such small submodel volumes the element size can be very fine without increasing the computational cost. For the studied geometries an element size of 1 mm is recommended to obtain convergence and produce high resolution in the strain predicted by the model.

The submodelling approach correlate well to physical tests. Comparison show that visual micro-damage in the polymer structure from tests can be predicted by submodelling in a more appropriate way than correlating it to the global shell model.

A script for automation of the submodelling approach has been developed containing modules for post-processing of the global model, submodelling and post-processing of the submodels. By using the scripted modules the total modelling time was reduced considerably compared to when carry out the submodelling steps manually. The script controls the submodelling procedure to a level where the users are still able to interact with the modelling and thereby can use their engineering judgements to verify the validity of the models.

References

[1] M. Oldenbo. *Dura CAE 2012-016-01 Comparison shell and solid GOR model,* Volvo Car Corporation, Göteborg, Sweden. 2012.

[2] J. Carlsson and M. Hammar. *Dura CAE 2013-084-02 Modelling manual for polymers,* Volvo Car Corporation, Göteborg, Sweden. 2013.

[3] H. Molker et al. 'Identifying failure initiation in automotive structures made of NCF reinforced composites for hot spot analysis'. English. In: *ECCM17 - 17th European Conference on Composite Materials* (2016).

[4] M. Oldenbo. *Dura CAE 2009-054-03 CAE Polymer guide,* Volvo Car Corporation, Göteborg, Sweden. version 3. 2014.

[5] L. Gigliotti and S. T. Pinho. 'Virtual Testing of Large Composite Structures: A Multiple Length/Time-Scale Framework'. English. In: *Journal of Multiscale Modellin, Imperial College Press* (2015).

[6] F. Larsson and K. Runesson. *The finite element method - Solid Mechanics.* English. Göteborg, Sweden: Chalmers University of Technology, 2015.

[7] T. P. Fries et al. 'Hanging nodes and XFEM'. English. In: *International Journal for Numerical Methods in Engineering* 86.4-5 (2011), pp. 404–430.

[8] Abaqus. *Abaqus Theory Guide - 6.6.2 Shell to solid constraint.* URL: `http://bobcat.nus.edu.sg:2080/v6.14/books/stm/default.htm?startat=ch06s06ath153.html` (visited on 23/02/2017).

[9] C. G. Dávila. 'Solid-to-shell transition elements for the computation of interlaminar stresses'. English. In: *Computing Systems in Engineering* 5.2 (1994), pp. 193–202.

[10] L. Gigliotti and S. T. Pinho. 'Multiple length/time-scale simulation of localized damage in composite structures using a Mesh Superposition Technique'. English. In: *Composite Structures* 121 (2015), pp. 395–405.

[11] T. Abbey. *Global-to-Local Modeling in FEA.* 2014. URL: `http://www.digitaleng.news/de/global-local-modeling-fea/` (visited on 23/01/2017).

[12] J. W. Huijin, C. Hoe and W. EE. Hua. 'Modelling solder joint reliability off BGA packages subjected to drop impact loading using submodelling'. English. In: *2002 Abaqus Users' Conference* (2002).

[13] J. M. Zarzalejos et al. 'Bolted Ribs Analysis for the ITER Vacuum Vessel using Finite Element Submodelling Techniques'. English. In: *Fusion Engineering and Design* 89.7-8 (2014), pp. 1790–1794.

[14] R. Nayak. *Submodeling Technique in Stress Analysis.* HCL Technologies. 2011. URL: `https://www.hcltech.com/sites/default/files/resources/whitepaper/files/2011/07/19/Submodeling_Technique_in_Stress_Analysis.pdf` (visited on 23/02/2017).

[15] R. Krueger and T. K. O'Brien. 'A shell/3D modeling technique for the analysis of delaminated composite laminates'. English. In: *Composites Part A* 32.1 (2001), pp. 25–44.

[16] Abaqus. *Abaqus Analysis User's Manual - 10.2.1 Submodeling: overview*. URL: http://abaqusdoc.ucalgary.ca/books/usb/default.htm?startat=pt04ch10s02aus58.html (visited on 23/01/2017).
[17] C. Klason et al. *Plaster: Materialval och Materialdata*. Swedish. 5. Stockholm: Sveriges verkstadsindustrier, 2001.
[18] J. Elmered. *Dura CAE 2005-015-06 Body and Closures - FE-Model Specification*. Volvo Car Corporation, Göteborg, Sweden. 2015.
[19] M. Oldenbo. *Dura CAE 2014-070-01 V541 UPV1 sillmoulding trunklid strength,* Volvo Car Corporation, Göteborg, Sweden. 2014.

Appendix

A Geometries and load cases

The three load cases used in the analyses are described below. One simplified geometry, *Reference load case* and two more complex geometries, *sillmouldings* to detect further difficulties in the implementation. The rear door sillmoulding is used in the correlation work, Section 5.

A.1 Reference load case

The reference load case geometry is shown in Figure A.1. This consists of a plate with a T-junction to a rib similar to what often is found in plastic components at VCC. The bottom plate is 400 × 160 mm and the rib is 120 mm high and 40 mm wide. Both the plate and the rib are modelled 3 mm thick, with a radius of 0.3 mm at the connection. The material used in the model is Acrylonitrile Butadiene Styrene (ABS), an amorphous thermoplastic polymer [17].

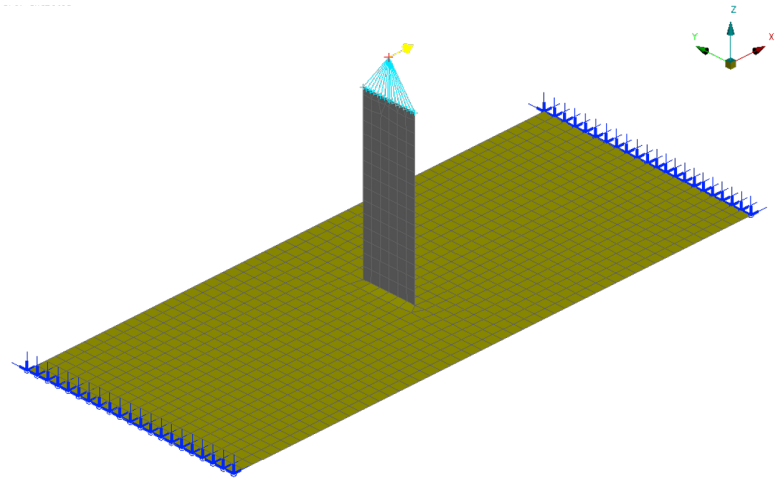

Figure A.1: The simplified load case (shell model) with applied load and boundary conditions.

The short sides of the bottom plate are fixed (all motions prevented) and a load of 10 N has been applied at the top of the T-junction parallel to the longest edge of the plate. The load, seen in Figure A.1, is applied at a node 27 mm above the geometry and coupled with rigid elements to the nodes at the top of the T-junction, this to make the load mesh independent. As the geometry is fairly small and has no complex details besides the radius at the T-junction this allows for meshing the total structure using both shell and solid elements. These models are used as references when creating, analysing and validating the submodelling approaches.

The global shell models are created using the *Mid. Surface*-tool in Ansa. This creates a surface centred in the cross section to the geometry's volume. According to VCC guidelines, T-junctions should be modelled using a smoother transition radius at the connection. Both this and the standard T-casting setting in Ansa is used to compare the differences, see Figure A.2. The shell elements used are of first order with 4 integration points. The solid models (both global models and

submodels) are modelled with a volume tetra mesh and a thin layer (0.001 mm) of membrane shells at the surfaces to get comparable strain result. According to VCC modelling guidelines shell elements should have a target length of 3 mm and solid elements a target length of 2 mm in more detailed models [2].

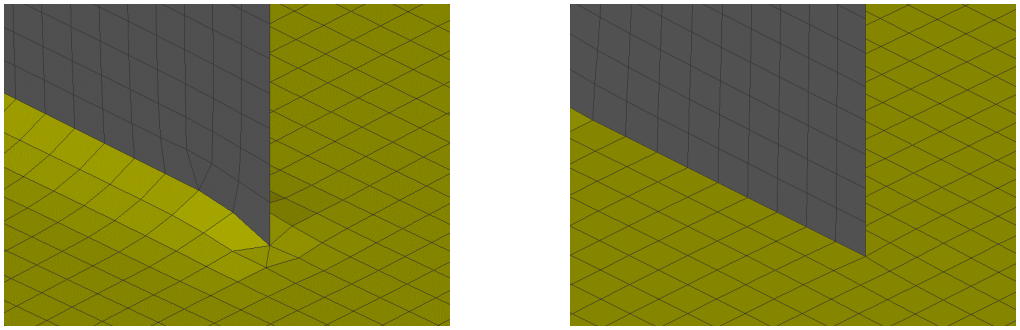

(a) Smooth T-junction (VCC standard) **(b)** Sharp T-junction

Figure A.2: 3 mm shell element mesh using two different types of T-junction treatment.

A.2 Trunk lid sillmoulding

The load case "Sillmoulding trunk lid strength" is a common engineering problem already taken into account at VCC today. The purpose of the load case is to validate the strength and stiffness in the trunk lid sill in the back end of the car, blue in Figure A.3. The component is loaded by a 1 kN force applied to a round specimen plate with a radius of 40 mm, red in Figure A.3. By moving the plate to other positions different load cases can be considered. However, in this report, only the position shown in the figure is used. The total FE-model used to evaluate this load case consist of the whole lower back end of the car body, modelled primarily with shells (3 - 8 mm) representing the mid-surfaces of the parts.

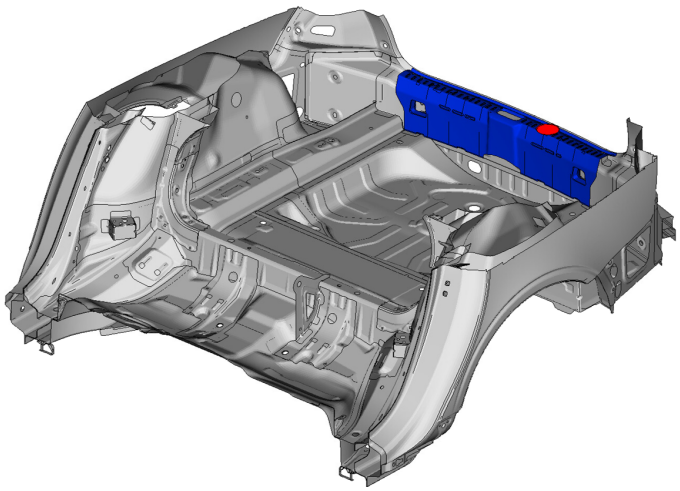

Figure A.3: Global FE-model of the back of the car used to evaluate strength in the sillmoulding (blue). The component is loaded vertical at the red mark.

The requirements for the trunk lid sillmoulding are stated as follows; the first principal strain should not exceed the design strain for the material and there should be no visual damage or deformation (maximum 5 mm deformation during loading and maximum 2 mm residual deformation). In a report, of an early design of the trunk lid sillmoulding, the component was marked as NOK as the first principal strain exceeded the allowable strain limit [19]. The sill is made of Polypropylene (PP), see Figure 7 with a design strain at 3% for short term loading [4].

A.3 Rear door sillmoulding

The structure visualised in Figure A.4 is used to validate that the rear door sillmoulding (yellow) fulfils its requirements on strength and stiffness. The analysis is very similar to the load case in Appendix A.2. A round specimen with a diameter of 75 mm is positioned and pushed vertical with a force of 1 kN at one of four different positions, representing that a person steps on the sill when entering or leaving the car. The sill is made of ABS-material, the same used in the reference load case and has been connected to the car body using several different kinds of clips. The FE-modelling of clips is difficult due to their non-linear stiffness responses. Often these are modelled using non-linear springs to represent the friction and contact behaviour in different directions when the clip is subjected to loading. In the global shell model used for correlation however solid clips are used. The T-ribs in the sillmoulding are 2 mm thick and modelled with a 1 mm shell mesh in the global FE-model.

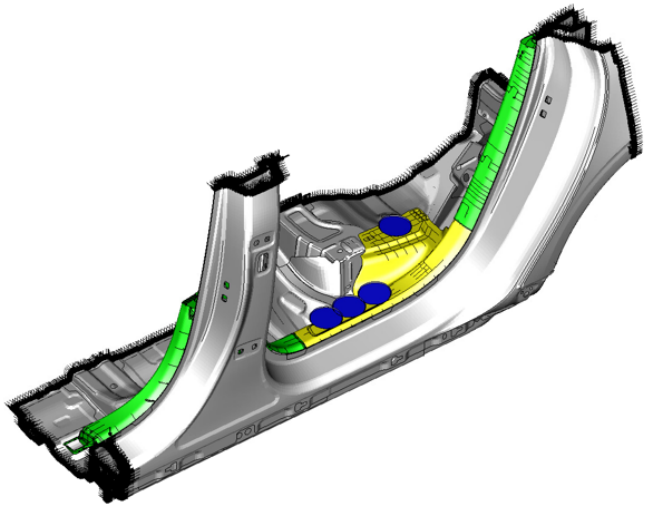

Figure A.4: Rear door sill marked in yellow and the four load positions marked in blue.

The predicted FE-model response for this load case is correlated to physical tests in Section 5. In the testing the same loading positions as in the FE-model are used, see left picture in Figure A.5. The middle picture in Figure A.5 shows the test setup located at load point 3. However, the correlation work was done after loading at position 4. In the test the displacement was measured vertically at the sensors, right photo in Figure A.5, which provided the force-displacement response for the considered location.

The test outcome indicated some critical areas in the rib-structure. The sillmoulding showed so called white marks from crazing on the radius for some of the T-junctions, see Figure 31. Also, crazing defects (micro cracks) had been initiated.

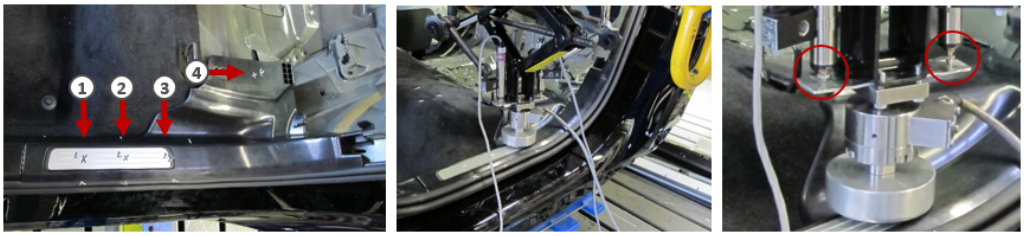

Figure A.5: Left: The four load points. Middle: Load setup located at load point 3. Right: Sensor positions.

B Meta hot-spot file

In the hot-spot file, generated from Meta, the following information is given;

- Files: File paths for the global model analysis. First row; file used for geometry (*.inp* or *.odb*). Second row; file used for result (*.odb*).
- Id: Element number at hot-spot in global model. Only used for naming. Can be changed but shall be unique for each hot-spot.
- pos: Global coordinates of hot-spot.
- value: Scalar value at the identified hot-spot.
- size: Submodel size. The radius in case of spheres.
- parts: Property id (PID) + name of the part in the submodel volume. In case of connections the connected parts are included as well.
- MID: Material id for the parts where the hot-spot appear.
- thickness: Shell thickness for the part where the hot-spot appear. If nodal thickness is used in the global model the maximum thickness of the parts inside the submodel volume is given.
- steps: Number of analysis steps in global simulation.

Listing 1: Hot-spot file example.

```
# File paths:
* /..../globalmodel.inp
* /..../globalmodel.odb
# Id, xpos, ypos, zpos, size, MID, thickness, steps, part, value
11,53.0,17.1,7.3,20,33410,2.5,3,['P7;PartName7', 'P9;Part9'],0.06
20,55.1,17.4,-7.9,24,33410,3.5,3,['P7;PartName7'],0.04
33,58.6,24.7,-7.9,20,33410,2.0,3,['P7;PartName7'],0.02
```

C Time and response differences

Table C.1: Reference load case results.

Model	Elements			Sim. time	First principal strain			Displacement	Evaluation
	Length	Type	Quantity	Seconds	Max	Point 1	Point 2	Max [mm]	OK/NOK
Global (shell)[6]	3mm	Shell (S4)	8206	1	1,035%	1,035%	0,733%	44,19	OK*
Global (shell)[7]	3mm	Shell (S4)	7770	2	1,034%	1,034%	0,698%	44,26	OK*
Global (sol)	3mm	C3D10, M3D6	172764	41	1,534%	1,048%	1,320%	44,89	OK
Global (sol)	2mm	C3D10, M3D6	438836	105	1,270%	1,056%	1,270%	44,90	OK
Global (sol)	1mm	C3D10, M3D6	3436828	1218	1,497%	1,053%	1,463%	45,02	OK
Global (sol)	1mm, refined	C3D10, M3D6	3714368	2223	1,650%	1,054%	1,637%	45,05	OK
Submodel	2mm	C3D10, M3D6	88834	30	1,213%	1,009%	1,213%	18,30[8]	OK
Submodel	1mm	C3D10, M3D6	702088	255	1,388%	1,010%	1,387%	18,32	OK
Submodel	1mm, refined	C3D10, M3D6	1030649	546	1,751%	1,006%	1,604%	18,31	OK

[6] Configuration (a) in Figure A.2.

[*] Assuming that Point 1 lies "outside" the radius area and that the true design criteria can be used.

[7] Configuration (b) in Figure A.2.

[8] Prescribed boundary condition.

D Further analyses and special cases

D.1 Output precision in global analysis

The output precision, i.e. the number of output decimal places, can be specified when solving a model. According to the Abaqus manual full output precision (maximal number of decimal places) should be used in the global analysis for submodel applications [16]. Figure D.1 shows the error in first principal strain when using full respectively single output precision, Equation 2 for the reference load case. The strain response differs only marginally (on the eighth to ninth decimal) at the driven boundaries. This is negligible in relation to the accuracy of the FE-solution and for the analyses of Point 1 and Point 2 in Section 4.1 these effects could not be distinguishable on the response. However, since a difference exists, even if very small, full output precision is recommended.

To use full output precision the global model is solved with the additional command;

abaqus [queue, version, etc.] job=global_model.inp output_precision=full

If full output precision is not used this is stated in the Abaqus *.pre*-file of the submodel solution.

$$\varepsilon_{1,\,\mathrm{diff}} = \varepsilon_{1,\,\mathrm{full\ precision}} - \varepsilon_{1,\,\mathrm{single\ precision}} \tag{2}$$

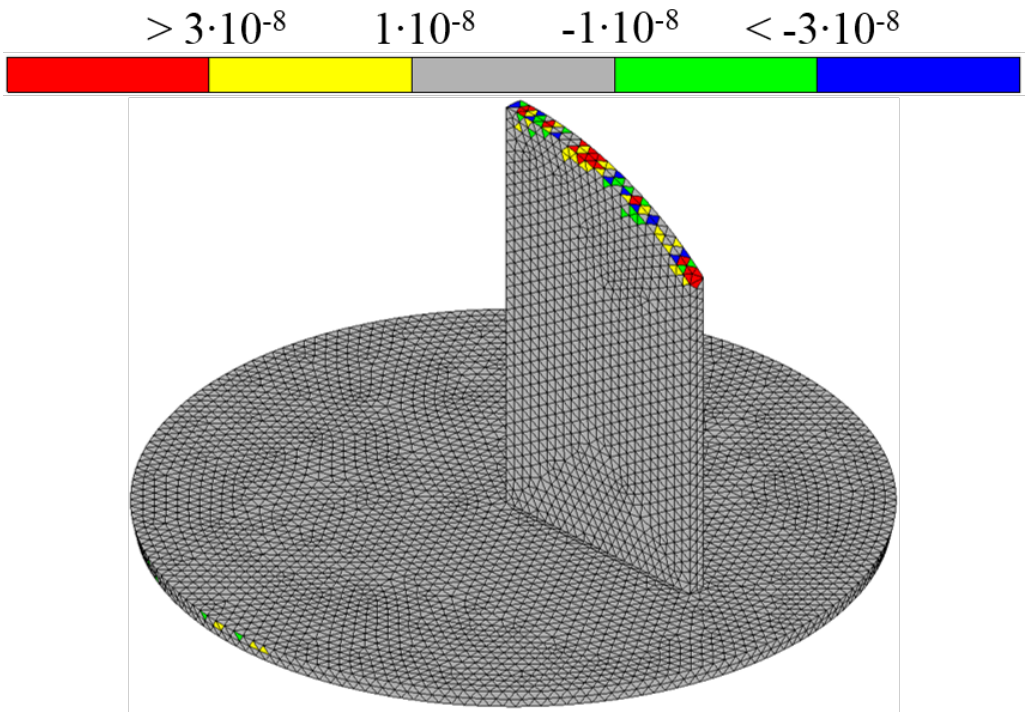

Figure D.1: Difference in first principal strain response using full respectively single output precision in global analysis, Equation 2.

D.2 Mesh convergence of trunk lid sillmoulding

For hot-spot A and E in the trunk lid (Figure 23) spherical submodel volumes with radius 20 and 30 mm respectively were created. The submodels were analysed using three different mesh setups (2, 1 and 0.5 mm element target length) as discussed in Section 4.2.3.1.

Figure D.2 and Figure D.3 illustrate the response patterns in addition to the ones already given in Section 4.2.3.1 while Table D.1 and Table D.2 gives the maximum strain levels in the hot-spot as well as the simulation times for each of the two cases. In general, smaller elements gave higher resolution on the strain response and the differences between adjacent elements were reduced. However, the tendency of a increasing maximum first principal strain was only observed for Model A. For 0.5 mm and 1 mm element meshes the maximum strains are thought to depend on the modelling approach using rigid elements. The small element size entails that the strain levels from the singular elements at the hole will effect surrounding elements, however the resolution of the strains becomes smoother. The 2 mm mesh is too coarse to obtain any detailed information regarding the submodel. For hot-spot A with submodel radius of 20 mm the simulation time is hardly affected by a refined mesh while for hot-spot E and radius 30 mm it soon became a significant time parameter to the total modelling time.

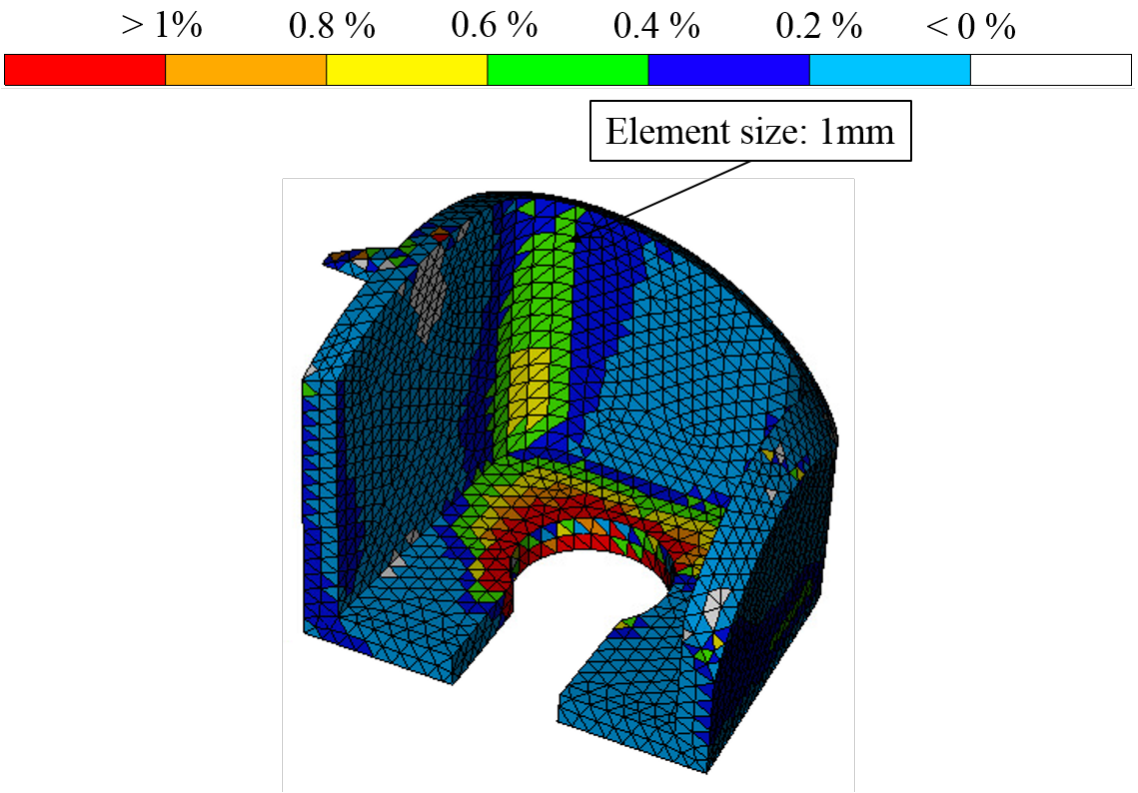

Figure D.2: First principal strain response pattern at hot-spot A using 1 mm element size.

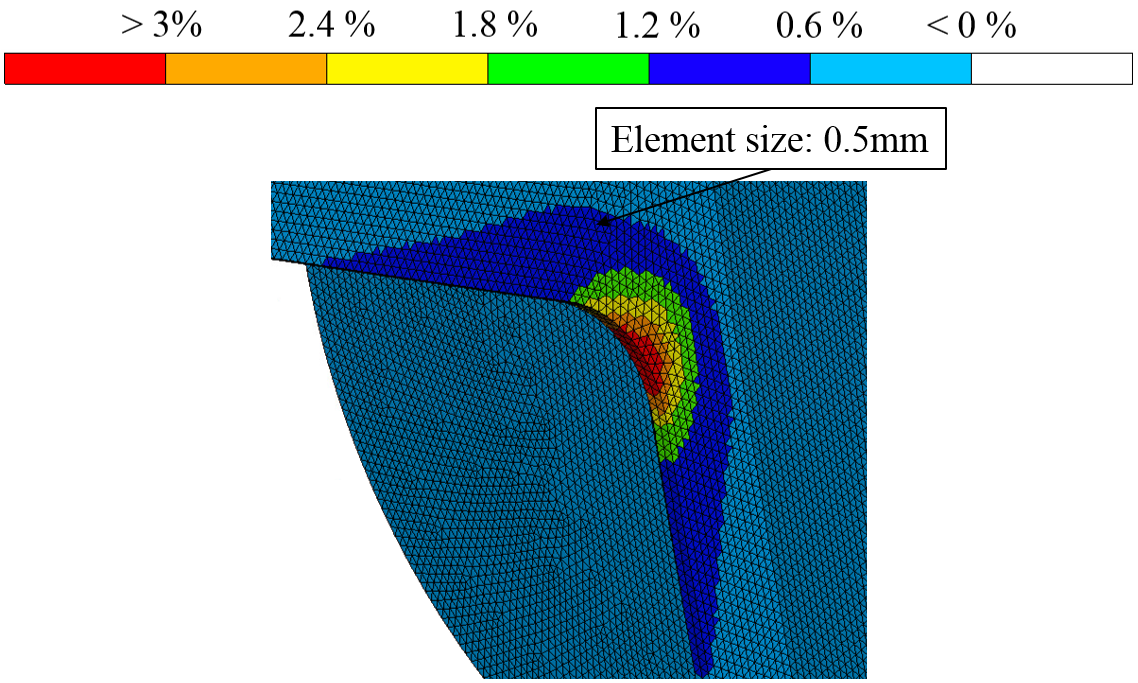

Figure D.3: First principal strain response patterns at hot-spot E using 0.5 mm element size.

Table D.1: Maximum first principal strain response and simulation time (wallclock time) for different mesh sizes used in trunk lid submodel A.

Element size	Elements	Sim. Time	Max strain*
2 mm	3442	4	0.98%
1 mm	36074	57	4.23%
0.5 mm	112216	214	7.65%

Table D.2: Maximum first principal strain response and simulation time (wallclock time) for different mesh sizes used in trunk lid submodel E.

Element size	Elements	Sim. Time	Max strain
2 mm	22029	15	3,794%
1 mm	176857	203	3,768%
0.5 mm	1372118	1699	3,799%

*Excluding the driven element set.

D.3 Submodel volume size in trunk lid sillmoulding

Tables D.3 and D.4 gives the maximum strain response for submodels of different size at two hot-spot locations in the trunk lid sillmoulding case. The submodel size was analysed in Section 4.2.3.2 and the error is plotted in Figure 29. For hot-spot E the response variation is small, Table D.3. Also, the hot-spot was not located close to a boundary. Hence, excluding driven boundary response from the result did not affect the evaluation. For hot-spot A the response the critical strain response is highly fluctuating, Table D.4.

Table D.3: Maximum first principal strain response for different submodel sizes (sphere radius) at hot-spot E. Relative error compared to largest volume (32 mm).

Radius [mm]	32	28	22	18	15	12	8	5
Max strain	3,85%	3,78%	3,72%	3,68%	3,68%	3,76%	3,44%	3,47%
Rel err.	-	-1,8%	-3,3%	-4,3%	-4,2%	-2,1%	-10,4%	-9,6%

Table D.4: Maximum first principal strain response for different submodel sizes (sphere radius) at hot-spot A. Relative error compared to largest volume (28 mm).

Radius [mm]:	28	22	18	15	12	8	5
	Inc. hole boundary elements						
Max strain.	10,99%	11,24%	10,27%	10,16%	10,74%	11,42%	9,14%
Rel err.	-	2,2%	-6,5%	-7,6%	-2,3%	3,9%	-16,8%
	Excl. hole boundary elements						
Max strain.	4,09%	4,14%	3,71%	4,82%	4,50%	3,18%	5,72%
Rel err.	-	1,2%	-9,5%	17,8%	10,0%	-22,4%	39,7%

D.4 Contact in vicinity of imposed boundary condition

When analysing the submodels created for the trunk lid sill one model, Model D in Figure 23, showed suspicious strain results in the rear part of the geometry. The strain levels in this part showed a strange pattern and also unrealistic high strain levels. This was not the case for the global model in the same area, cf. Figure 22. The identified reason for this behaviour is a consequence of the models location within the global model. Model D shows a strange behaviour that appears just were the loading of the global model was imposed. In Figure D.4 the downward pushing specimen, causing the loading of the component has been included for illustration. As the load is applied to the model this causes contact and to some degree also penetration between the two components.

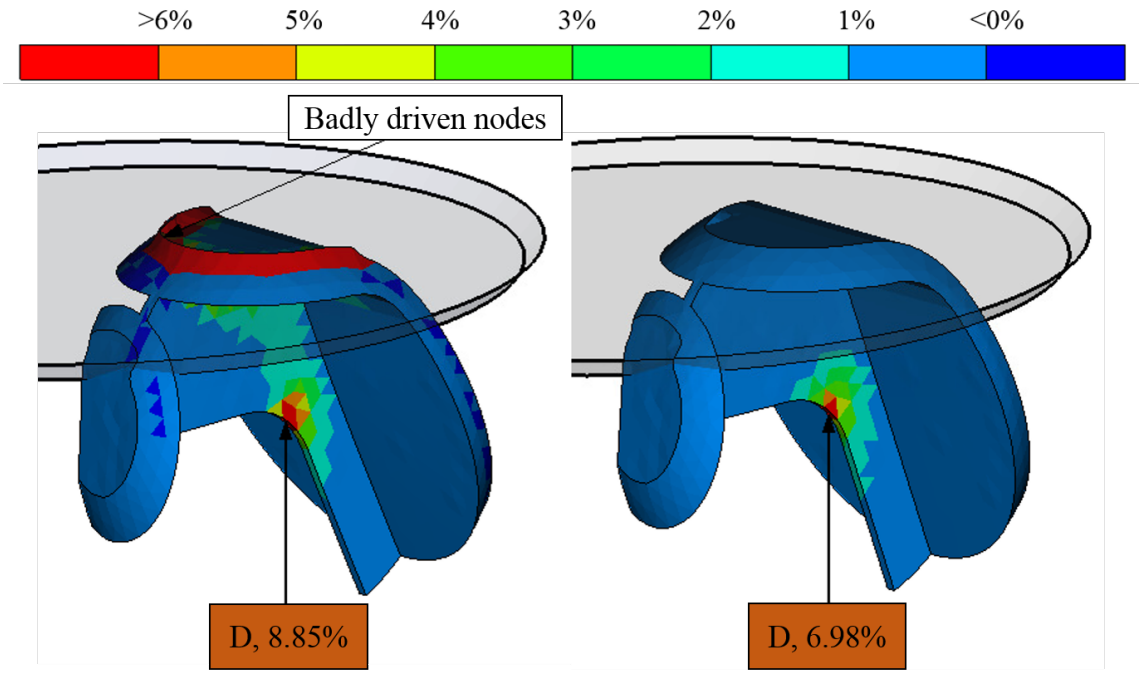

Figure D.4: Left: Load specimen connected to driven node set. Right: Load specimen excluded from driven node set.

It appears that this contact and penetration causes problems when the FE-solver (Abaqus) tries to automatically decide which node displacements from the global model that shall be applied to the driven set of nodes in the submodel. It is a question how to impose boundary conditions on this submodel. Shall the results from the sillmoudling, the loading plate or both be used? In this case some of the driven nodes at the trunk lid boundary connects and are imposed by the global displacement results for the load specimen instead. These nodes in the submodel will then continue to follow the path of the load specimen which under unloading causes unrealistic high strains.

This phenomena could be solved by excluding the loading specimen to be a part of possible displacements that can be imposed on the submodel boundary. This is done by manually defining the global element set when creating the submodel analysis in Ansa (Ansa: *Deck - Abaqus - Auxiliaries - Submodel - Global elset*). In such way the submodel can only be driven by the response from the trunk lid sill and not from the loading specimen of the global model. The result is seen in Figure D.4 (right) where the unphysical phenomenon does not appear anymore. The maximum critical strain level for the hot-spot is now 6.98% (D* in Table 2).